

Development of radiative cooling and its integration with buildings: A comprehensive review

Jianheng Chen, Lin Lu *

Department of Building Services Engineering, The Hong Kong Polytechnic University, Hong Kong, China



ARTICLE INFO

Keywords:
 Radiative cooling
 Spectral selectivity
 Daytime cooling
 Building cooling
 Cool roof

ABSTRACT

Radiative cooling is an appealing heat exchange form based on thermal radiation from terrestrial objects to outer space, which can be potentially applied to numerous cooling applications for system performance improvement without energy input. Due to the poor solar reflective ability of previous cooling materials, radiative cooling technology has been largely limited to nocturnal cooling for several decades. Thanks to the recent successful development of highly efficient selective and broadband thermal emitters either backed with high solar reflective metal films or intrinsically equipped with excellent solar reflectance properties, the daytime radiative cooling has been practically fulfilled, which is arousing worldwide research interests. Notably, the emerging nanophotonics or metamaterials-based fabrication approaches are widely reported with the prominent ability to tailor spectral properties for sub-ambient cooling enhancement. Porous polymer-based scalable paints with micro-and nanopores are also developed with substantial daytime cooling capacities by considerably backscattering sunlight and emitting thermal radiation. This work comprehensively reviews the latest progress on radiative cooling regarding its theoretical fundamentals, material designs and a variety of novel applications with a special focus on building-integrated cooling performance improvement. Considering the preceding extensive research on cool roofs with remarkable potential for real-world implementations, radiative roof cooling has been discussed in terms of cool roof-based heat transfer models, thermal and energy performance, and economic and environmental benefits. Lastly, research prospects of the radiative cooling technology are envisaged to provide insight for further investigation.

1. Introduction

Due to the rapid development of global economy and urbanization, energy consumption is dramatically escalating to satisfy increasing demands of human beings in pursuit of quality life. Among all energy users, building sectors as the main energy consumers, as a rule of thumb, approximately take up 40% of primary energy consumption worldwide (Lu et al., 2016), of which over 65% is consumed by HVAC systems contributing to 1/3 of CO₂ emissions (Hernández-Pérez et al., 2014). Hence, as a large energy consumption industry, energy savings in buildings are crucial in counteracting energy-intensive development modes to achieve a sustainable society. Building cooling which is the main driver of peak electricity demands is a fundamental requirement fulfilled by air-conditioning systems to obtain indoor thermal comfort. However, the current predominant vapor compression-based air conditioning systems are massive energy consumers which involve the usage of refrigerants to arouse environmental concerns. Due to the growing

awareness of energy efficiency (Zhao et al., 2019d), seeking for an alternative passive cooling method as a supplementary or self-sustained power supply system to achieve building cooling is of great significance for efficient energy utilization in buildings.

Radiative cooling is a ubiquitous process in which a surface conducts heat exchange with outer space by thermal radiation. Cooling states of an object are established by continuously emitting more thermal radiation into the universe than it absorbs from the atmosphere. Technically, the earth has a surface temperature around 300 K which is much higher than the outer space of around 3 K (Fixsen, 2009). Thereby, if the enormous temperature difference between the earth and the universe is efficiently utilized, continuous passive radiative cooling for objects on the earth can be potentially realized. The appealing value of radiative cooling is the reduced surface temperature for a variety of materials without requiring any energy input (Sun et al., 2017b), which may tremendously change our current energy exploitation methods towards self-sustained and pollution-free power supply pathways. Nevertheless, many technical obstacles should be overcome before the practical

* Corresponding author.

E-mail address: vivien.lu@polyu.edu.hk (L. Lu).

Nomenclature	
<i>c</i>	Speed of light in vacuum, m/s;
<i>g</i>	Acceleration of gravity, N/kg;
<i>G</i>	Incident solar radiation, W/m ² ;
<i>E</i>	Pumping power of a lift pump, W;
\hat{h}	Planck's constant, J·s;
<i>h</i>	Heat transfer coefficient, W·m ⁻² ·K ⁻¹ ;
<i>H</i>	Height of water being lifted from the ground pump to the cooling panels, m;
<i>HG</i>	Daily average downward heat gains through a sunlit roof, J/m ² ;
<i>I</i>	Spectral radiation intensity, W·sr ⁻¹ ·m ⁻³ ;
<i>k</i>	Heat conductivity coefficient, W·m ⁻¹ ·K ⁻¹ ;
<i>k_B</i>	Boltzmann constant, J/K;
<i>P</i>	Power emitted out or absorbed by a surface, W/m ² ;
PWV	Precipitable water vapor, mm;
<i>Q</i>	Volumetric water flow rate of a pumping system, m ³ /h;
<i>R</i>	Thermal resistance, m ² ·K·W ⁻¹ ;
SR	Cool roof solar reflectance;
SRI	Cool roof solar reflectance index;
TE	Cool roof thermal emittance;
<i>t</i>	Atmospheric transmittance in zenith direction;
<i>T</i>	Temperature, °C;
ΔT	Temperature reduction, °C;
<i>U</i>	Overall heat transfer coefficient, W·m ⁻² ·K ⁻¹ ;
<i>V</i>	Voltage, mV;
<i>Greek letters</i>	
α	Solar absorptance;
β	Solar reflectance;
γ	Infrared transmission;
δ	Thickness of a roof layer, m;
ε	Thermal emittance;
η_c	Overall transmission efficiency;
η_p	Pump efficiency;
η_m	Mechanical transmission efficiency;
<i>η_e</i>	Electric motor efficiency;
θ	Zenith angle, °;
λ	Wavelength, m;
ρ	Water density, kg/m ³ ;
<i>Subscripts</i>	
a	Atmosphere;
amb	Ambient;
AM1.5	Air mass 1.5 solar spectrum;
atm	Atmospheric radiation;
black	Standard black surface;
BB	Blackbody;
c	Convective heat transfer;
ce	External convective heat transfer;
cell	Solar cell;
ci	Internal convective heat transfer;
cold	Cold photonic surface;
e	External roof surface;
eq	Equilibrium;
hemispherical	Incidence at hemispherical direction;
hot	Hot photonic surface;
i	Internal roof surface;
indoor	Indoor air;
max	Maximum output;
net	Net cooling power;
nonrad	Non-radiative heat transfer;
normal	Incidence at normal direction;
o	Overall heat transfer between a roof and ambient air;
pump	Lift pump;
r	Radiative surface;
rad	Radiative power;
re	External radiative heat transfer;
ri	Internal radiative heat transfer;
roof	Multilayered roof structures;
Sun	Incident solar radiation;
white	Standard white surface;

radiative cooling can be fulfilled. Actually, besides the thermal radiation emitted out into the universe, an object placed on the terrestrial environment proactively interacts with numerous factors including, for instance, the incident solar irradiance, the incoming atmospheric radiation, the convective and conductive heat exchange with stochastic external environment. Apparently, the radiative cooling capacity could be enhanced provided that the radiative power from the object should take dominance in the miscellaneous heat exchange components as stated above. Otherwise, the radiative cooling power is easily counteracted by external factors. Limited to the insurmountable challenge of solar absorption during the daytime, the research on radiative cooling, which though could be traced back to past several decades, was mainly focused on the nocturnal cooling (Hanif et al., 2014). Many materials with the high thermal emissivity were developed for nocturnal cooling tests in pursuit of positive cooling powers (Eriksson et al., 1984; Granqvist, 1981; Hjortsberg and Granqvist, 1980), which were basically smaller than 100 W/m², thus entailing large surfaces for implementations to achieve required cooling capacities. Until recently, thanks to the advent of nanophotonic designs backed with a silver film, the first practical daytime radiative cooling has been experimentally fulfilled by using seven alternating layers of hafnium oxide (HfO₂) and silica (SiO₂) on top of a silver substrate (Raman et al., 2014). With the solar reflection of 97%, the photonic structure could achieve a sub-ambient temperature of 4.9 °C and a cooling power of 40.1 W/m². Subsequent more promising structure was reported by Zhai et al (Zhai et al., 2017) with a cost-

effective, glass-polymer hybrid metamaterial to achieve the cooling power of 110 W/m². Based on such scalable-manufactured metamaterial, some demonstrative cooling applications were proposed, including the cooled water of 10.6 °C below ambient (Zhao et al., 2019c) and the integration with air-conditioning systems to provide cooling energy for a residential building (Zhang et al., 2018). Numerous daytime radiative cooling materials were subsequently reported.

The integration of radiative cooling with building systems as the passive cooling method has the large potential for widespread applications in the years ahead in light of the increasingly full-fledged daytime cooling materials. In addition to the combination of cooling materials with air-conditioning systems, the most direct and appealing way is to use them as building roof surfaces, which are the main recipient of the solar radiation and contribute noticeable heat gains into the indoor environment. For instance, roof surface accounts for 14% of cooling loads for low-rise buildings (Konopacki et al., 1997). Gao. et al. (2017) also indicated the roof top heat transmission accounts for 5%-10% of overall energy consumption in buildings and over 40% in top floors. Hence, using radiative cooling materials as roof coatings or membranes will make a big difference to building energy savings. In terms of the radiative roof cooling, cool roof scheme (Akbari and Levinson, 2008) is a widely acknowledged practice to achieve passive cooling in buildings. Its benefits regarding the thermal and energy performance as well as economic and environmental impacts have been extensively studied. However, the current cool roof products are mainly composed of bulk

materials without strong solar reflectance to maximize the cooling capacity. Thereby, the utilization of new daytime radiative cooling materials with much higher solar reflectance and thermal emittance than conventional coatings as cool roof surfaces will achieve more potential benefits in buildings.

In light of the escalating development of radiative cooling materials and studies, this paper presents a comprehensive review on the development of radiative cooling technology from the fundamentals of radiative cooling to the progress of materials development and various potential applications. The paper also sheds light on the future prospects over key technical issues aiming to promote radiative cooling for large-scale applications in buildings. The uniqueness of this work can be summarized as follows: 1) considering the rapid advancement in radiative cooling research, a bunch of latest reports on this field regarding new cooling materials and novel designs, applications and studies are critically reviewed and comprehensively analyzed; 2) the paper fundamentally conducted detailed parametric analyses on radiative cooling performance based on the established theoretical model. Specifically, the impacts of water vapor contents on the radiative cooling power in extremely dry, and hot and humid climate regions are calculated and analyzed respectively; 3) different radiative cooling designs with testing conditions and the infrared emittance at hemispherical or normal incidence or under a certain incident angles are newly summarized and tabulated for a fair comparison of the cooling performance; 4) a variety of hybrid novel radiative cooling applications in buildings are summarized. Specifically, theoretical discussions from the perspective of energy use were presented regarding the practical feasibility of pumping water through the plumbing systems to achieve cooling power in high-rise buildings; 5) more advanced explorations of radiative cooling are discussed, such as adaptive radiative cooling designs with tuneable optical properties, and radiative cooling-assisted thermoelectric applications; and 6) the application performance of radiative roof cooling combined with latest daytime radiative cooling materials is newly summarized and discussed, and a bunch of cool roof-based heat transfer models are thoroughly reviewed with or without the consideration of spectrally selective properties.

2. Fundamentals of radiative cooling

2.1. Model establishment

Considering a flat surface shown in Fig. 1, the heat exchanges between the radiative surface and the time-varying external environment mainly involve the components of absorbed incident solar radiation P_{sun} , incoming atmospheric radiation P_{atm} , outgoing radiative power from the surface P_{rad} and the non-radiative heat exchange P_{nonrad} between the surface and surrounding atmosphere (Hossain and Gu, 2016; Zeyghami et al., 2018; Zhao et al., 2019a). A detailed analysis on the above power components will illustrate the basic fundamentals of radiative cooling.

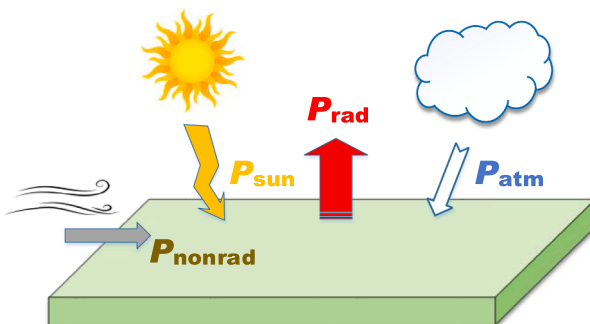


Fig. 1. Radiative surface heat exchanges, including the absorbed solar radiation P_{sun} , downward atmospheric radiation P_{atm} , outgoing radiative power P_{rad} and non-radiative heat exchange P_{nonrad} .

Assuming a radiative surface with the temperature T and emittance $\epsilon_r(\lambda, \theta)$, when the surface is exposed to external environment with the air temperature T_{amb} under direct sunlight, it interacts with varying solar irradiance, atmospheric thermal radiation as well as the flowing air. When considering all the interacting components, the net cooling power P_{net} of the radiative surface can be decided as:

$$P_{\text{net}}(T) = P_{\text{rad}}(T) - P_{\text{atm}}(T_{\text{amb}}) - P_{\text{Sun}} - P_{\text{nonrad}} \quad (1)$$

where the power radiated out from the surface is:

$$P_{\text{rad}}(T) = 2\pi \int_0^{\pi/2} \sin\theta \cos\theta d\theta \int_0^{\infty} I_{\text{BB}}(T, \lambda) \epsilon_r(\lambda, \theta) d\lambda \quad (2)$$

Here,

$I_{\text{BB}}(T, \lambda)$ is the spectral radiance of a blackbody at the temperature T , $\text{W}\cdot\text{sr}^{-1}\cdot\text{m}^{-3}$:

$$I_{\text{BB}}(T, \lambda) = \frac{2\hat{h}c^2}{\lambda^5} \frac{1}{e^{\hat{h}c/\lambda k_B T} - 1} \quad (3)$$

Here,

\hat{h} is the Planck's constant, $6.62607004 \times 10^{-34} \text{ J}\cdot\text{s}$;

k_B is the Boltzmann constant, $1.38064852 \times 10^{-23} \text{ J/K}$;

c is the speed of light in vacuum, $3.0 \times 10^8 \text{ m/s}$;

λ is the wavelength, m .

According to Kirchhoff's law of thermal radiation which relates the absorptance of a surface equivalently to its emittance, the absorbed incident atmospheric radiation is defined as:

$$P_{\text{atm}}(T_{\text{amb}}) = 2\pi \int_0^{\pi/2} \sin\theta \cos\theta d\theta \int_0^{\infty} I_{\text{BB}}(T_{\text{amb}}, \lambda) \epsilon_r(\lambda, \theta) \epsilon_a(\theta, \lambda) d\lambda \quad (4)$$

where, $\epsilon_a(\theta, \lambda)$ is the angle and spectrum dependent emittance of the atmosphere, which can be approximated by (Granqvist, 1981):

$$\epsilon_a(\theta, \lambda) = 1 - [1 - \epsilon_a(0, \lambda)]^{1/\cos\theta} = 1 - [t(\lambda)]^{1/\cos\theta} \quad (5)$$

where, $\epsilon_a(0, \lambda)$ is the spectrum dependent emittance in the normal direction, and θ is the zenith angle. $t(\lambda)$ is the atmospheric transmittance in the zenith direction which is heavily dependent on the local atmospheric conditions (Berk et al., 2006).

The absorbed solar power by the radiative surface is expressed as:

$$P_{\text{Sun}} = \int_0^{\infty} I_{\text{AM1.5}}(\lambda) \epsilon_r(\lambda, \theta_{\text{Sun}}) d\lambda \quad (6)$$

where, $I_{\text{AM1.5}}(\lambda)$ is the AM 1.5 spectrum radiation (NREL-ASTM, 2003).

The non-radiative power is defined as:

$$P_{\text{nonrad}}(T, T_{\text{amb}}) = h_{\text{nonrad}}(T_{\text{amb}} - T) \quad (7)$$

where, h_{nonrad} is the combined non-radiative heat transfer coefficient to capture the collective effects of conductive and convective heat transfer between the radiative surface and surrounding air. The empirical correlations related to local wind speeds can be adopted to calculate the coefficient (Zeyghami et al., 2018).

2.2. Calculation description

For the detailed analysis of the above model, the solar irradiance of AM 1.5 spectrum and the atmospheric transmittance from (Gemini Observatory, 2019) are utilized for calculations as presented in Fig. 2. The wavelength from 8 to 13 μm is regarded as the atmospheric transparency window which coincidentally falls within the peak spectral irradiance of the blackbody with the temperature of 30 °C. The

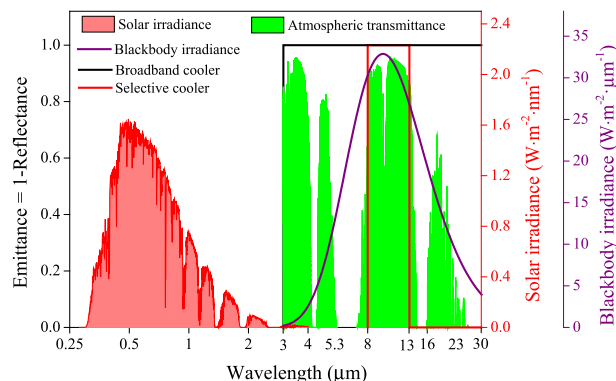


Fig. 2. Solar irradiance, atmospheric transmittance and spectral emittance of two ideal radiative coolers.

characteristic elucidates the potential of terrestrial objects to radiate more heat than it absorbs into the outer space for passive cooling (Hossain and Gu, 2016).

Two ideal radiative coolers are assumed, namely broadband and selective coolers respectively. The broadband cooler has a unity emittance within the entire infrared wavelength except for the solar spectrum from 0.3 to 3 μm . While the selective cooler is only emissive within the atmospheric transparency window from 8 to 13 μm . The two coolers are totally solar reflective and the main difference is the infrared emittance profiles. Considering radiative cooling are particularly desirable in tropical zones where ambient air temperature remains slightly changed, the ambient temperature is taken as 30°C (Ao et al., 2019).

2.3. Parametric analysis

The developed heat transfer model correlates the net cooling power $P_{\text{net}}(T)$ of a radiative cooler with its surface temperature T . The positive net cooling power can be achieved if the radiative cooler under ambient temperature emits more heat into outer space than it gains from the solar and atmospheric radiation as well as non-radiative heat transfer. When the net cooling power $P_{\text{net}}(T)$ reduces to zero, the radiative cooler can thereby reach a minimum steady-state equilibrium temperature T_{eq} . Thus, two pivotal parameters are adopted in the following analysis to evaluate the cooling performance of radiative coolers, namely the achievable net cooling power $P_{\text{net}}(T = T_{\text{amb}})$ when coolers' temperatures reach the ambient air, and the equilibrium temperature $T_{\text{eq}}(P_{\text{net}} = 0)$ when the net cooling power reduces to zero.

2.3.1. Impacts of radiative coolers

The impacts of two ideal radiative coolers with different spectral properties on achievable net cooling powers and equilibrium temperatures are presented in Fig. 3. The results were obtained by considering radiative power emitted from the coolers and the absorbed atmospheric radiation in Equation (1).

Due to the different spectral properties across the infrared wavelength ranges, two radiative coolers exhibit different characteristics regarding the achievable net cooling powers and equilibrium temperatures. The selective cooler with the narrowest emissive wavelengths exhibits extraordinary ability to achieve the minimum equilibrium temperature (239.8 K) whilst simultaneously present the lower achievable net cooling power (119.5 W/m²) at the ambient temperature. The narrow absorptive wavelength of the selective cooler corresponds to a smaller radiative power P_{rad} emitted from the surface for heat dissipation. However, it also absorbs the least incoming atmospheric radiation P_{atm} from the atmosphere to be counteracted by P_{rad} so as to ensure a positive net cooling power P_{net} . Under low temperature ranges, the radiative power P_{rad} is significantly restrained according to Stefan–Boltzmann law which defines the power radiated out from a

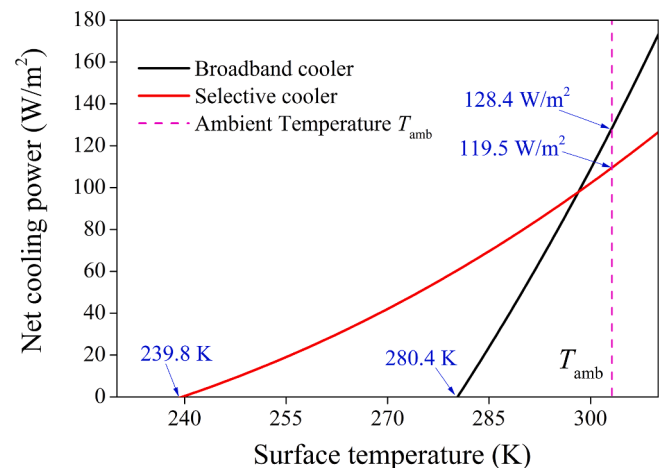


Fig. 3. Net cooling power versus surface temperature.

blackbody is directly proportional to the fourth power of its temperature. Therefore, the selective cooler with the stringent emissivity within the atmospheric window is preferable in the sub-ambient application scenarios. While the broadband cooler with the widest emissive wavelength from 3 μm to ∞ shows the maximum achievable net cooling power (128.4 W/m²) at the ambient temperature while conversely the least capacity to achieve minimum equilibrium temperature (280.4 K). Because of the largest absorption of the atmospheric radiation for the broadband cooler, the overwhelmingly reduced outgoing radiative power under low temperature ranges is largely offset by the absorbed atmospheric radiation, thus undermining its cooling potential under sub-ambient temperatures. By and large, the spectrally emissive properties arising from different radiative coolers can exert great impacts on radiative cooling potential, and they are applicable to different scenarios either for pursuing extremely low temperatures or large cooling powers.

2.3.2. Influence of other factors

In addition to the above-mentioned spectrum properties of radiative coolers, external factors directly interacting with coolers, such as the non-radiative heat exchanges and the atmospheric conditions, will also exert significant impacts on the achievable cooling potential (Zhao et al., 2020c). The non-radiative heat coefficient h_{nonrad} is a pivotal parameter to represent extents of heat exchanges between radiative coolers and external environment. The corresponding impacts are illustrated in Fig. 4 (a) regarding the equilibrium temperatures of two coolers which are assumed with the additional 3% solar absorption. Since the sub-ambient scenarios are more desired in pursuit of radiative cooling, the results thereby present the sub-ambient temperature ranges. The achievable equilibrium temperature differences $T_{\text{amb}} - T_{\text{eq}}$ of two radiative coolers decrease rapidly as h_{nonrad} increases, indicating the existence of h_{nonrad} will significantly weaken the radiative cooling capacity. The higher external air temperature will drive the heat flow from outside into radiative coolers, which requires to be counteracted by the radiative power and thus reduces the overall cooling potential. As h_{nonrad} increases, the characteristics of both coolers become gradually indistinctive as illustrated in Fig. 4(a) with h_{nonrad} over 10 W·m⁻²·K⁻¹. Therefore, it is worth noting that to maximize radiative cooling potential under sub-ambient scenarios, the inhibition of non-radiative heat transfer is necessary in practical experimental studies. To this end, infrared transparent polyethylene (PE) films which are almost transparent to all wavelengths can be utilized as effective shields to fulfil the purpose (Ao et al., 2019; Catalanotti et al., 1975; Diatezua et al., 1996; Hu et al., 2017; Kou et al., 2017; Li et al., 2019b; Raman et al., 2014; Suichi et al., 2018; Trombe, 1967; Zeyghami et al., 2018; Zhao et al., 2019a). Additionally, a corrugated high-density polyethylene film (Nilsson et al., 1985) and a polyethylene mesh structure (Gentle et al., 2013) were also

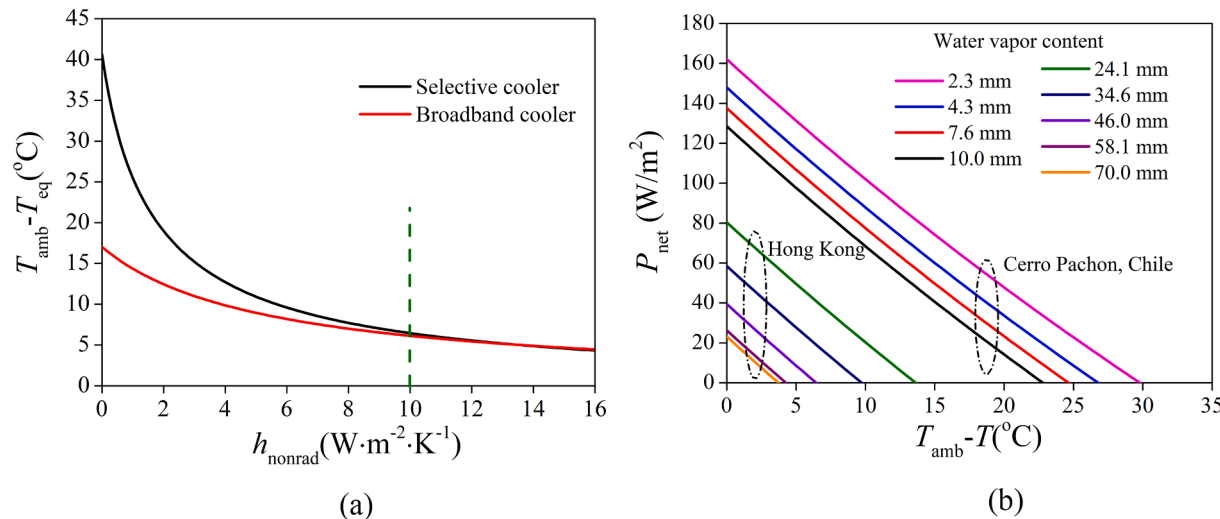


Fig. 4. (a) Influence of non-radiative heat coefficient h_{nonrad} on equilibrium temperature difference $T_{\text{amb}} - T_{\text{eq}}$. (b) Influence of atmospheric conditions on net cooling power P_{net} and sub-ambient temperature $T_{\text{amb}} - T$.

proposed atop radiative coolers. While to overcome the degradation issues, Bathgate and Bosi (2011) proposed a more robust zinc sulphide based convection cover which is impervious to damages of external environment with better mechanical properties.

The atmospheric transmittance which is highly related to the local precipitable water vapor (PWV) contents (Han et al., 2020; Harrison, 1981; Hossain and Gu, 2016; Khedari et al., 2000; Landro and McCormick, 1980; Liu et al., 2019a; Zhao et al., 2019b; Zhao et al., 2019c) will exert impacts on the atmospheric radiation as shown in Equations (4) and (5) and the net cooling power (Fig. 4 (b)). The increase in water vapor contents will reduce the atmospheric transmittance and thus augment its infrared absorption and emittance, the increase of which corresponds to a reduced net cooling power as illustrated in Equation (1). Specifically, when the water vapor content increases from 2.3 mm to 4.3, 7.6, 10 mm in Cerro Pachon (Gemini Observatory, 2019), the net cooling power of the broadband cooler reduces by 13.1 (8%), 24.5 (15.1%), 33.6 (20.7%) W/m^2 , respectively, whilst the achievable sub-ambient equilibrium temperature reduces by 3 (10.1%), 5.2 (17.4%), 7.1 (23.8%) °C, respectively. However, it should be noted that for tropical or subtropical regions with hot and humid climate patterns, the PWV levels can be much higher than those of the exceedingly dry climate in Cerro Pachon to severely limit the radiative cooling performance. To this end, five cases of water vapor contents in Hong Kong with the typical humid subtropical climate were adopted for further analysis between the PWV levels and the net radiative cooling power (Fig. 4(b)). The acquisition of PWV contents in certain days was from the Upper Air Data Soundings (University of Wyoming, 2020) which contains daily data from Hong Kong's King's Park Meteorological Station. The atmospheric transmittance corresponding to different PWV levels was calculated by the MODTRAN model (Berk et al., 2006). As illustrated in Fig. 4(b), the large PWV levels substantially undermine the achievable radiative cooling power. Particularly, as the PWV content increases from 24.1 mm to 34.6, 46.0, 58.1 and 70.0 mm, respectively, the net cooling power diminishes 21.8 (27.2%), 40.9 (50.9%), 54.0 (67.3%) and 57.2 (71.3%) W/m^2 respectively. It is worth noting that PWV contents can be considerably high in hot months with 59.5, 60.8, 61.6, 48.7 mm in average from June to September, respectively (Fig. 5). Such high humidity with consequent strong downwelling atmospheric radiation will dramatically counteract the radiative power and thus inhibit the realization of radiative cooling. As evident in Fig. 4(b), during the hot months in the subtropical city of Hong Kong, the ideal broadband cooler without any solar absorption and convective heat transfer only achieves the net cooling power ranging from 20 to 40 W/m^2 . If the unavoidable

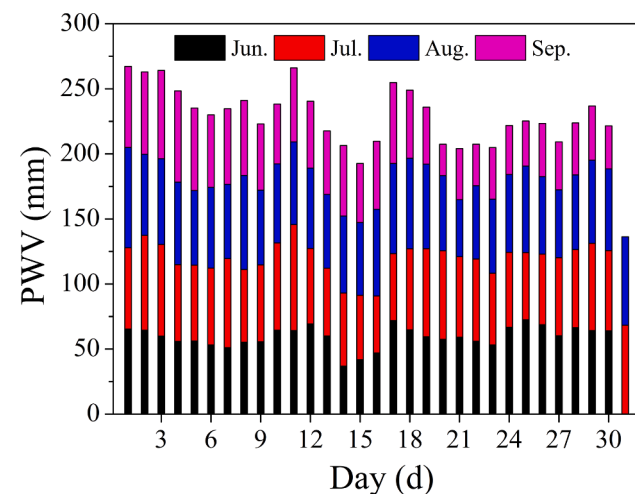


Fig. 5. The precipitable water vapor (PWV) contents in Hong Kong (year 2019).

convective heat and minor solar absorption are considered in practical scenarios, the radiative cooling may be barely achieved. Hence, radiative cooling capacities are heavily dependent on local atmospheric conditions and entail detailed evaluation for a certain radiative cooler under specific climates.

3. Material designs and applications of radiative cooling

Radiative cooling materials and structure designs have been investigated extensively including both nighttime and daytime cooling applications. Starting from several centuries ago, nocturnal radiative cooling has been explored to cool buildings and desalinate water (Granqvist, 1981; Granqvist and Hjortsberg, 1981). The realization of nocturnal radiative cooling dated back to ancient utilizations of the clear sky as the heat sink to make basins for ice productions (Bainbridge and Haggard, 2011; Zeyghami et al., 2018). Although some designs composed of bulk or composite materials (Sun et al., 2017b), such as polymer films, pigments and inorganic materials, exhibit adequate selective thermal emission, they are almost poorly solar reflective, thus largely restricting their applications with quite limited daytime radiative cooling capability, albeit remarkable nighttime radiative cooling

based on these designs is widely demonstrated. Thanks to the recent innovation in the fabrication of nanophotonics-based materials backed with a silver film to fulfil the spectral requirements of both high solar reflectance and selective thermal emittance within the atmospheric transparency window, the practical daytime radiative cooling has been experimentally realized (Raman et al., 2014). Subsequently, the advances in nano-and microparticle-doped and polymer-based material designs also progressively exhibit satisfactory daytime radiative cooling performance.

3.1. Designs with limited daytime radiative cooling capability

3.1.1. Polymer films

Polymer film-based material designs are pioneers for nocturnal radiative cooling (Zhao et al., 2019a). Trombe (1967) was the first to suggest the use of polymers for radiative cooling and show how the atmospheric window could be harnessed for the radiative cooling purpose. The typical polymer films used at the early stage mainly included polyvinyl chloride (PVC) (Trombe, 1967), polyvinyl fluoride (PVF) (Bartoli et al., 1977; Catalanotti et al., 1975) and polymethylpentene (TPX) (Grenier, 1979) thin films coated on aluminum (Al) substrates. Specifically, the PVF based polymer film coated on an evaporated aluminum plate exhibited selective thermal absorption within the wavelength from 9 to 13 μm , which could achieve the sub-ambient temperature reduction of 12°C (Catalanotti et al., 1975). Polyvinylidifluoride (PVDF) was also adopted as spectrally selective material for radiative cooling applications (Matsuta et al., 1987) and the cooling performance was better than non-selective surfaces. Other polymer-based materials include polymethyl methacrylate (PMMA) (Muselli et al., 2002), modified polyphenylenoxid (PPO) resin (Meir et al., 2002). Until recently, two new polymer film-based materials were proposed. Hu et al. (2016) combined the polyethylene terephthalate (PET) material with a titanium-based solar absorber to manufacture a composite surface, which exhibited the experimental net cooling power of 23.4 and 50.3 $\text{W}\cdot\text{m}^{-2}$ for overcast and clear nights. Czapla et al. (2017) developed the PDMS-based selective emitter with or without SiC nanoparticles embedded, which analytically presented a sub-ambient temperature reduction of 12 °C under a clear night. Polymer films demonstrate the advantage of being produced on a massive scale for commercial applications.

3.1.2. Pigmented paints

Pigmented paints which mainly contain titanium dioxide (TiO_2) layers coated on aluminum substrates with strong thermal selective emissivity were also reported with the nocturnal cooling capacity. Harrison et al. (1978) reported a white paint containing TiO_2 on an Al plate which could achieve a sub-ambient temperature of 15 °C under a clear sky. Michell and Biggs (1979) further investigated the TiO_2 -based white paint on a galvanized steel, which obtained the cooling power of 22 $\text{W}\cdot\text{m}^{-2}$ when the roof temperature maintained at 5 °C. Kimball (1985) compared the TiO_2 -based white paint with the black paint and obtained the temperature reduction of 11 °C for white paints. Due to the enhanced absorption by SO_4 stretching vibrations, the component of BaSO_4 was added to TiO_2 -based paints (Orel et al., 1993) aiming to achieve improved effects. Consequently, the temperature reduction of the pigment with BaSO_4 was increased by 3.2 °C when compared to that only containing TiO_2 . Actually, pigmented paints which are the most widespread and effective cooling design at present are more flexible for roof retrofits and outperform polymer films for practical applications. The common practice of adding rutile TiO_2 as the white pigment in paints has long been employed to achieve high thermal emittance (Council and Directory, 2019; Wojtysiak and Butler, 2009). A typical white paint usually contains TiO_2 pigments which impart a near-unity and broadband emittance of ~ 0.95 on paints (Yu et al., 2016). However, due to the intrinsic absorption of the ultraviolet ($\lambda \sim 0.3\text{--}0.4 \mu\text{m}$) and violet ($\lambda \sim 0.4\text{--}0.41 \mu\text{m}$) light and near-infrared solar absorption (λ

$\sim 0.7\text{--}2.5 \mu\text{m}$) by polymer binders, the optimized solar reflectance is below 0.86 for the best TiO_2 -based paints (Mandal et al., 2020), which tremendously inhibits the realization of daytime radiative cooling of the pigmented paints under direct sunshine. In addition to the TiO_2 -based white paints, pigments with non-white colors are also desired to stay cooler under the sun for esthetics, which can be fulfilled either by using cool colored materials with the high near-infrared (700–2500 nm) reflectance (Synnefa et al., 2007b) or by utilizing the phenomenon of fluorescence (Berdahl et al., 2016), where based on the fluorescent emission to transport radiant energy the ruby fluorescence with efficient emission in the deep red ($\sim 694 \text{ nm}$) and near infrared (700–800 nm) was utilized to reduce the surface temperature of non-white colored materials. The blue pigments as infrared phosphors containing Ca, Sr, and Ba variants fluorescing in the near-infrared at 909, 914, and 948 nm were also found with strong fluorescence to enhance cooling of sunlit surfaces (Berdahl et al., 2018).

3.1.3. Inorganic materials

Inorganic cooling materials mainly comprised silicon-related films coated on aluminum substrates, for instance, silicon based components (SiO , Si_3N_4 , SiO_2 , SiC). Additionally, Berdahl et al. (1984) utilized the magnesium oxide (MgO) coated on an aluminum foil to obtain a nocturnal net cooling power of $85 \text{ W}\cdot\text{m}^{-2}$, exhibiting a better cooling performance than PVF materials. Granqvist et al. (1980) studied the property of SiO film deposited on an aluminum substrate and discovered a strong IR emission within the wavelength of 8–13 μm centered at 10 μm under the optimal layer thickness of 1 μm . The radiator experimentally achieved the cooling temperature of 14 °C below the ambient. In the following study, the Si_3N_4 film based radiator was proposed with a stronger and better thermal selectivity (Granqvist et al., 1982). Similarly, the thin film of silicon oxynitride ($\text{SiO}_{0.6}\text{N}_{0.2}$) with the thickness of 1.34 μm evaporated on an aluminum substrate (Eriksson et al., 1984), and the SiO_2 and $\text{SiO}_{0.25}\text{N}_{1.52}$ bilayers coated on an aluminum substrate (Eriksson et al., 1985) were also reported with selective thermal emissions. Diatezua et al. (1996) proposed three kinds of silica and silicon oxynitride-based multilayers for passive cooling applications and predicted temperature drops ranging from 48 to 56 °C with cooling power varying from 118 to 125 W/m^2 . The nanoparticles with 5% SiC and 5% SiO_2 by volume in polyethylene films deposited on an aluminum substrate (Gentle and Smith, 2010) presented good selective thermal emissions due to the surface phonon resonance. The film experimentally achieved the nocturnal sub-ambient temperature of 17 °C which was consistent with the calculated value of 18.5 °C.

3.1.4. Gaseous material designs

Due to the molecular vibration and rotation yielding spectrally selective infrared emission, gases can also be utilized for radiative cooling. The ethylene (C_2H_4) gas was first demonstrated with the cooling capacity to achieve a sub-ambient cooling temperature of 10 °C (Hjortsberg and Granqvist, 1981). The 2 cm thick ammonia (NH_3) gas slab was proposed with a sub-ambient temperature of 15 °C (Lushiku et al., 1982). Furthermore, the mixture of the 25% C_2H_4 and 75% $\text{C}_2\text{H}_4\text{O}$ (Lushiku and Granqvist, 1984) could achieve the cooling power of $85 \text{ W}\cdot\text{m}^{-2}$ under the slab thickness of 5 cm. However, limited to the encapsulation requirement, gases-based cooling is precluded from practical applications. The aforementioned designs with limited daytime but remarkable nighttime radiative cooling capability are summarized in Table 1.

3.2. Designs with adequate daytime radiative cooling capability

Over 10% of absorbed solar energy may offset the produced radiative cooling power (Zeyghami et al., 2018). Hence, eliminating solar absorption is significant to realize adequate daytime radiative cooling. Two configurations of radiative coolers were proposed for solar blocking (Fu et al., 2019). The first approach is to prevent solar radiation from

Table 1

Summary of typical designs with limited daytime but remarkable nighttime radiative cooling capability.

Materials/structures	Spectral property	Testing conditions	Cooling performance	Schematic diagram
Polymer films				
Polyvinyl fluoride (PVF) film coated on an aluminum substrate (Catalanotti et al., 1975)	$\varepsilon \sim 0.8\text{--}0.9$ (8–13 μm) $\varepsilon \sim 0.15$ (outside 8–13 μm)	$T_{\text{amb}} \sim 280.6$ K (Experiment)	$\Delta T \sim 12$ °C	
Polymethylpentene (TPX) film coated on an aluminum substrate (Grenier, 1979)	$\varepsilon \sim 0.8\text{--}1$ (8–13 μm)	–	$P_{\text{net}} \sim 32$ W/m ²	
Polyethylene terephthalate (PET) film applied on a solar absorber (Hu et al., 2016)	$\varepsilon \sim 0.74\text{--}0.83$ (8–13 μm)	On clear and overcast nights in July to cool water with the flowrate of 0.012 kg/s, in Hefei, China (Experiment)	$P_{\text{net}} \sim 50.3$ W/m ² (clear night); $P_{\text{net}} \sim 23.4$ W/m ² (overcast night)	
Polydimethylsiloxane (PDMS) thin film coated on an aluminum substrate (Czapla et al., 2017)	$\varepsilon_{\text{hemispherical}} \sim 0.5\text{--}0.96$ (8–13 μm)	$h_{\text{nonrad}} = 2$ W m ⁻² K ⁻¹ ; Under a clear night sky (Calculation)	$\Delta T \sim 12$ °C	
Pigmented paints				
TiO ₂ -based white paint coated on an aluminum plate (Harrison and Walton, 1978)	$\varepsilon \sim 0.92$ (8–13 μm)	$T_{\text{amb}} \sim 25$ °C; Absolute humidity ~ 2.5 g/m ³ ; Under a clear sky in Calgary, Canada (Experiment)	$\Delta T \sim 15$ °C	
TiO ₂ -based white paint coated on a galvanized steel (Michell and Biggs, 1979)	$\beta \sim 0.86$; $\varepsilon \sim 0.78\text{--}0.94$ (5–25 μm)	$T_{\text{amb}} \sim 9\text{--}13.7$ °C; Relative humidity $\sim 53\text{--}74\%$; Under a clear night sky (Experiment)	$\Delta T \sim 5$ °C; $P_{\text{net}} \sim 22$ W/m ²	
TiO ₂ -based white paint on an aluminum fin plate (Kimball, 1985)	$\varepsilon \sim 0.92$ (8–13 μm)	$T_{\text{amb}} \sim 20\text{--}30$ °C; Under a clear night sky (Experiment)	$\Delta T \sim 11$ °C	
BaSO ₄ and TiO ₂ as components in white paints applied in aluminum panels (Orel et al., 1993)	$\varepsilon \sim 0.9$	$T_{\text{amb}} \sim 15.4$ °C; Under a humid night sky (Experiment)	$\Delta T \sim 10$ °C	
Inorganic materials				
SiO-based film on an aluminum substrate (Granqvist and Hjortsberg, 1980, 1981)	$\varepsilon \sim 0\text{--}0.9$ (8–13 μm) at 15° angle of incidence	$T_{\text{amb}} \sim 10\text{--}13$ °C; Relative humidity $\sim 80\text{--}95\%$; A clear night in Gothenburg, Sweden (Experiment)	$\Delta T \sim 14$ °C; $P_{\text{net}} \sim 61$ W/m ²	
Si ₃ N ₄ thin film coated on an aluminum substrate (Granqvist et al., 1982)	$\varepsilon \sim 0.41\text{--}0.98$ (8–13 μm)	–	–	
MgO film coated on an aluminum foil (Berdahl, 1984)	$\varepsilon_{\text{normal}} \sim 0.91$ (8–14 μm)	$T_{\text{amb}} \sim 15$ °C; A night under a dry atmospheric condition (Experiment)	$P_{\text{net}} \sim 85$ W/m ²	
SiO _{0.6} N _{0.2} -based film evaporated on an aluminum substrate (Eriksson et al., 1984)	$\varepsilon \sim 0.43\text{--}0.99$ (8–13 μm) at 45° angle of incidence	$T_{\text{amb}} \sim 12.3$ °C; Relative humidity $\sim 83\%$; A clear night at Gothenburg, Sweden (Experiment)	$\Delta T \sim 16$ °C	
SiO ₂ and SiO _{0.25} N _{1.52} -based bilayers coated on an aluminum substrate (Eriksson et al., 1985)	$\varepsilon \sim 0.44\text{--}0.92$ (8–13 μm) at 45° angle of incidence	–	–	

(continued on next page)

Table 1 (continued)

Materials/structures	Spectral property	Testing conditions	Cooling performance	Schematic diagram
SiO ₂ and silicon oxynitride multilayers deposited on an aluminum-coated glass substrate (Diatezua et al., 1996)	$\epsilon \sim 0.45\text{--}0.98$ (8–13 μm) at 45° angle of incidence	$T_{\text{amb}} \sim 27^\circ\text{C}$; No non-radiative exchanges (Calculation)	$\Delta T \sim 56^\circ\text{C}$; $P_{\text{net}} \sim 119 \text{ W/m}^2$	
Crystalline SiC and SiO ₂ nanoparticles mixed in polyethylene films deposited on an aluminum substrate (Gentle and Smith, 2010)	$\epsilon \sim 0.8\text{--}1$ (8–12 μm) at incident angles of 0–70°	$T_{\text{amb}} \sim 17^\circ\text{C}$; Water vapor pressure: 1.8 mm; $h_{\text{nonrad}} \sim 2 \text{ W m}^{-2} \text{ K}^{-1}$; (Calculation)	$\Delta T \sim 18.5^\circ\text{C}$	
Gaseous material designs				
Ethylene (C_2H_4) gas slab (Hjortsberg and Granqvist, 1981)	$\epsilon \sim 0\text{--}0.77$ (8–13 μm)	$T_{\text{amb}} \sim 5^\circ\text{C}$; Relative humidity ~ 40%; Slab thickness: 10 cm; In Gothenburg, Sweden (Experiment)	$\Delta T \sim 10^\circ\text{C}$	
Ammonia (NH_3) gas slab (Lushiku et al., 1982)	$\epsilon \sim 0.17\text{--}0.8$ (8–13 μm)	$T_{\text{amb}} \sim 15^\circ\text{C}$; Slab thickness: 2 cm; $h_{\text{nonrad}} \sim 1 \text{ W m}^{-2} \text{ K}^{-1}$; (Calculation)	$\Delta T \sim 15^\circ\text{C}$	
Mixture of C_2H_4 and $\text{C}_2\text{H}_4\text{O}$ gases slab (Lushiku and Granqvist, 1984)	$\epsilon \sim 0\text{--}0.85$ (8–13 μm) for C_2H_4 ; $\epsilon \sim 0\text{--}0.82$ (8–13 μm) for $\text{C}_2\text{H}_4\text{O}$	$T_{\text{amb}} \sim 15^\circ\text{C}$; Slab thickness: 5 cm with 25% C_2H_4 and 75% $\text{C}_2\text{H}_4\text{O}$; $h_{\text{nonrad}} = 1 \text{ W m}^{-2} \text{ K}^{-1}$; (Calculation)	$\Delta T \sim 20^\circ\text{C}$; $P_{\text{net}} \sim 85 \text{ W/m}^2$	

reaching coolers by using IR transparent solar reflective materials atop selective IR emitters. Such approach entails simultaneous high solar reflectance and IR transmittance for the covering materials. Several earlier trials were reported by doping inorganics into polyethylene films as shied covers, including TiO₂ pigments and carbon particles (Andretta et al., 1981), ZnS (Nilsson and Niklasson, 1995; Nilsson et al., 1992), semiconductors of PbS and PbSe (Dobson et al., 2003) and CdTe (Bellattar et al., 2005), which barely demonstrated daytime cooling performance in most cases due to the difficult spectral requirement of both high solar reflectance and IR transmittance. While recent advances in materials have successfully exhibited the daytime cooling by these designs (Leroy et al., 2019; Torgerson and Hellhake, 2020). Another novel design is to utilize back solar reflectors on the bottom of solar transparent IR selective emitters, which has seen considerable development thanks to the advent of nanophotonics or metamaterials-based fabrication methods to engineer IR emitters with spectrally selective properties. In terms of the back solar reflectors, metals with a large extinction coefficient are regarded as excellent solar reflective materials, such as, silver (Ag) with a high solar reflectance of 0.97 for full wavelength ranges (Palik, 1998). Moreover, some non-silvered novel designs by using micro-and nano-pores in polymer materials to simultaneously backscatter sunlight and emit thermal radiation were also demonstrated with adequate daytime radiative cooling potential (Mandal et al., 2018b; Mandal et al., 2020).

3.2.1. Nanophotonic materials

Unlike bulk materials with intrinsic optical properties, photonic structures can be tailored with strongly and strictly selective thermal emission. If combined with a solar reflector, the radiative power emitted from the new structures can hopefully exceed the incident solar and atmospheric radiations, thus achieving net cooling powers. With the recent advances in the nanofabrication technology (Li and Fan, 2018), the nanophotonic-based radiative cooling materials have been successfully fabricated to overcome the insurmountable barrier of daytime solar

absorption. The first practical daytime radiative cooling was experimentally achieved based on a one-dimensional (1-D) planar photonic structure which comprises 7 multilayers of hafnium oxide (HfO_2) and silica (SiO_2) atop a silver substrate (Raman et al., 2014). To explore the extreme temperature reduction through radiative cooling, an experiment was further devised with a sunshade to largely block incident sunlight (Chen et al., 2016). Combined with the radiative cooler consisting of silicon nitride (Si_3N_4), amorphous silicon (Si) and aluminum (Al) layers deposited atop a Si wafer, the average and maximum sub-ambient temperatures of 37.4 °C and 42.2 °C were reported. Since Al_2O_3 turns out to be highly absorptive around the wavelength of 10 μm , Kecebas et al. (2017) substituted the component of HfO_2 layer in (Raman et al., 2014) with TiO_2 and further replaced the top layer with Al_2O_3 . The new design enhanced the cooling power from 40 to 100 W/m^2 . More complicated multi-layer dielectric micro-pyramid structure with a total of 19 alternating layers of aluminum oxide (Al_2O_3) and silica (SiO_2) deposited on a silver layer was proposed (Wu et al., 2018), which analytically achieved the cooling power of 122 W/m^2 and the equilibrium temperature of 253 K. 1-D planar nanophotonic structures were also developed for thermoelectric generation (Mu et al., 2019), solar cells cooling (Li et al., 2017) or color preserving applications (Li et al., 2018), and the related material fabrication methods include simulated annealing (Boudet et al., 1996), needle optimization (Tikhonravov et al., 2007), jump method (Li et al., 2009), memetic algorithm (Shi et al., 2018) to precisely control the layer thickness for maximizing spectral properties (Zhao et al., 2019a).

In addition to 1-D planar nanophotonic cooling materials which require strict controls on the thickness of each layer, the spectrally thermal selectivity can also be tailored through artificially fabricated microstructures, like plasmonic structures (Thongrattanasiri et al., 2012; Yan et al., 2013; Zhan et al., 2012), metallic photonic crystals (El-Kady et al., 2008; Fleming et al., 2002; Hossain et al., 2010), and metamaterials (Cui et al., 2014; Cui et al., 2011; Liu et al., 2010; Ma et al., 2013; Xiong et al., 2013). Based on the concepts of nanophotonics, a 2-D

photonic crystal comprising quartz and SiC was developed with selective thermal radiation, below which lies a dielectric reflector composed of multilayers of MgF₂ and TiO₂ on a Ag substrate for minimizing solar absorption (Rephaeli et al., 2013). The radiative cooler which could be produced through the roll-to-roll nanoimprint lithography was able to theoretically achieve a net cooling power over 100 W/m². Hossain et al. (2015) developed the metal-dielectric conical metamaterial (CMM) pillars consisting of aluminum (Al) and germanium (Ge)-based alternating layers with the IR emittance up to 90% within the wavelength from 8 to 13 μm. The radiator had a nocturnal cooling power of 116.6 W/m² and a sub-ambient temperature of 12.2 °C. If combined with a IR transmitting photonic solar reflector with 3% of solar absorption on top of the CMM emitter, the diurnal sub-ambient equilibrium temperature of 9 °C could be analytically achieved. Aimed at reducing large-scale fabrication cost by using UV photolithography or nanoimprint lithography, Zou et al. (2017) proposed a two-layer metasurface composed of phosphorous-doped n-type silicon and silver, which exhibited the minimum sub-ambient temperature reduction of 10.29 °C (nighttime) and 7.36 °C (daytime), respectively. Additionally, another metasurface-based radiative cooler made of Al-doped ZnO (AZO) conducting oxides was developed, below which lies an optical solar reflector with dielectric SiO₂ as the spacer and Al as the back reflector (Sun et al., 2018). The metareflector could achieve the thermal emittance of 0.79 and solar absorption of 0.16 for spacecraft cooling. Main obstacles inhibiting large-scale applications of 2-D photonic microstructure radiators are the complex fabrication methods. Moreover, the requirement for the strict spectral selectivity and strong IR emittance is still a challenge.

3.2.2. Nano-and microparticle-based materials

In comparison to bulk materials, nanoparticles or microspheres exhibit spectrally different properties due to microscopic structures. For instance, SiO₂-based bulk materials exhibit phonon-polariton resonances resulting in high spectral reflection. However, SiO₂-based nanoparticles turn out to have remarkable absorption within the same wavelengths (Zhao et al., 2019a). Hence, nanoparticles or microspheres enable to exhibit novel spectral characteristics to be utilized for radiative cooling. Polar dielectric resonant nanoparticles embedded in polymers have previously been reported with the radiative cooling capacity in (Gentle and Smith, 2010) and (Yu et al., 2016), and an experimental daytime radiative cooling was demonstrated by a scalable-manufactured glass-polymer hybrid metamaterial (Zhai et al., 2017), which contains SiO₂-based microspheres distributed randomly in polymethylpentene (TPX). The thermal emittance over 0.93 within the atmospheric transparency window was achieved and the cooling power of 93 W/m² under incident sunlight was reported. However, the role of TPX matrix in contributing to the spectral emittance remains unexplored. Based on the metamaterial (Zhai et al., 2017), a hybrid diurnal cooling module integrated with air-conditioning systems for residential buildings was proposed with detailed analysis on the energy savings and economic benefits in a typical two-floor single-family house (Zhang et al., 2018). Likewise, a novel application based on the same kind of material has been designed (Zhao et al., 2019c) to cool water to 10.6 °C below the ambient around noon under direct sunlight, which presented an appealing approach towards energy savings and efficiency improvement in buildings.

Actually, titanium dioxide (TiO₂) nanoparticles with high solar reflective ability are commonly adopted in white acrylic paints to increase surface solar reflectance. The increase of particle sizes of TiO₂ in pigments could decrease the coatings' solar and visible light reflectance (Song et al., 2014) and the optimum TiO₂ particles' size is ~ 200 nm (Berdahl and Bretz, 1997), which coincides with the mean particle size of the conventional TiO₂ (Berdahl and Bretz, 1997; Brady and Wake, 1992). To realize daytime radiative cooling, a nanoparticle doped double-layer coating was further developed which comprised acrylic resin with TiO₂ embedded as the top layer for solar reflection and carbon

black particles as the bottom layer for thermal emission (Huang and Ruan, 2017). With the optimum TiO₂ particles' radius size of 0.2 μm, >90% of solar radiation can be reflected. Based on the obtained spectral properties, a diurnal net cooling power of 100 W/m² was predicted. Moreover, a double-layer coating was proposed by (Bao et al., 2017) based on highly scalable nanoparticles consisting of packed TiO₂ particles as the top layer for solar reflection and SiC or SiO₂ nanoparticles as the bottom layer for thermal emission. With the solar reflectivity over 90.7% and thermal emittance within the atmospheric window of 90.11%, the designed structure could theoretically achieve the daytime sub-ambient temperature of 5°C. Furthermore, the low-cost random photonic silica microspheres were developed by minimizing the photon transport mean free path to adjust the spectral absorption (Atiganyanun et al., 2018). The new coating which could be applied in a paint format experimentally cooled a black substrate to 12 °C below the ambient under sunlight.

3.2.3. Polymer-based materials

Considering the large-scale manufacturability, polymer-based radiative cooling materials have also attracted wide attention. A birefringent polymer from a commercial manufacturer comprising alternating layers of polyethylene terephthalate (PET/ECDEL) with the total thickness of 67 ± 4 μm was utilized for an experimental daytime radiative cooling demonstration (Gentle and Smith, 2015). By combining a bottom silver layer for solar reflection, an appealing cooling capacity of 2 °C below the ambient was experimentally achieved without shield covers under the solar radiation of 1060 W/m². In comparison to a commercially available white paint, a temperature reduction of 11 °C was reached by the polymer which can be produced on a large scale for roof applications. A polydimethylsiloxane (PDMS) film (100 μm thick) as the top layer and a silver film (120 nm thick) as the bottom reflector were coated onto a fused silica wafer (500 μm thick) to form a polymer mirror (Kou et al., 2017), which acted as a near-ideal reflector in the solar spectrum and a blackbody in the mid-infrared wavebands. The polymer mirror experimentally obtained the temperature reductions of 8.2 °C (daytime) and 8.4 °C (nighttime) below the ambient with the estimated net cooling power of 127 W/m² outperforming complex nanophotonic materials for power generation. More explorations were reported on the development of polymer-based cooling materials. The multilayers of poly (methyl methacrylate) (PMMA) and SiO₂ deposited on an aluminum mirror was developed with the solar reflectance of 0.89 and selective thermal emittance of 0.72, which reduced the surface temperature of 3.4 °C below a bare aluminum mirror (Suichi et al., 2018). However, due to the narrowed atmospheric window caused by the high humidity, no practical sub-ambient cooling was observed. Notably, a novel hierarchically porous polymer coating made of 300 μm thick poly(vinylidene fluoride-cohexafluoropropene) (P(VdF-HFP)_{HP}) was promisingly fabricated (Mandal et al., 2018b) by using air voids to replace pigments in cool roof paints, which exhibited excellent daytime radiative cooling capacity with the sub-ambient temperature of 6 °C and cooling power of 96 W/m². Since the existing micro-and nano-pores in the coating simultaneously backscatter incident sunlight and emit thermal radiation, the P(VdF-HFP)_{HP} films with ~ 50% porosity and thickness ≥ 300 μm have a hemispherical solar reflectance of 0.96 and long-wave infrared thermal emittance of 0.97 without the requirement of Ag as the back reflector. It is worth mentioning that the toxic solvent of acetone used in the preparation of the precursor solution is not eco-friendly. Substitutions of such materials with water-based fluoropolymer variants would make paints more sustainable (Mandal et al., 2020).

More recently, Leroy et al. (2019) developed the polyethylene aerogel (PEA) which exhibited high solar reflection (92.2% at 6 mm thick), good infrared transparency (79.9%) and low thermal conductivity (28 mW·m⁻¹·K⁻¹) as the nonmetallic solar reflector. When integrated with a commercially available selective emitter as the bottom layer, the daytime cooling power of 96 W/m² and sub-ambient temperature of 13 °C were experimentally demonstrated under the average solar irradiance of

936 W/m². Similarly, an all-polymer filter with a high solar reflectance and low-wave infrared transparency was developed by uniformly distributing highly size-selective lossless air pores in polyethylene (Torgerson and Hellhake, 2020). The measured optical properties show an ~ 95% solar reflectivity and ~ 75% infrared transmission in the atmospheric transparency window, allowing for the underlying emitter to radiate heat into cold sky to achieve cooling performance.

3.2.4. Other radiative cooling designs

Additionally, there are some new emerging material designs for radiative cooling and thermal management. Recently, a wood-based structural material has been developed through the delignification and densification process (Li et al., 2019b). The cooling wood with a mechanical strength of 404.3 MPa comprises cellulose nanofibers that are capable of backscattering solar irradiance and strongly emitting mid-infrared radiation. The radiative cooling powers of 63 W/m²(nighttime) and 16 W/m² (daytime) were experimentally achieved, resulting in an average value of 53 W/m² throughout 24 h. Correspondingly, sub-ambient temperatures reached over 9 °C (nighttime) and 4 °C (midday) with building energy savings ranging from 20% to 60% using the cooling wood as exterior surfaces in 16 cities of America. A SiO₂ mirror emitter with the broadband thermal emission deposited on a silver layer was proposed with daytime cooling potential to achieve a sub-ambient temperature of 5.9 °C under the dry sky whilst it was barely effective for moist weather conditions (Zhao et al., 2019b). Two broadband radiators with specular (ultra-white glass-plated silver) and diffuse surfaces (zinc phosphate sodium (NaZnPO₄) particles on an aluminum substrate) have been developed (Ao et al., 2019). The specular and diffuse surfaces experimentally achieved sub-ambient temperatures of 9.8 °C and 7.3 °C at nighttime, while the values reduced to 2.5 °C and 1.5 °C during the daytime, respectively. A porous anodic aluminum oxide (AAO) membrane was chemically fabricated and deposited on an aluminum substrate, which demonstrated a sub-ambient temperature of 2.6 °C and a cooling power of 64 W/m² (Fu et al., 2019).

Through the above analysis, it can be found that metals like silver or aluminum-based substrates as back solar reflectors are commonly adopted in daytime radiative cooling designs. However, it should be noted that in reality, radiative coolers have some surface roughness, and silver deposited on them is not smooth. Moreover, sputtering or vapor deposition processes usually result in imperfect films, and thus silver usually has a reflectance closer to 0.94–0.95. Aluminum, whose solar reflectance is approximate to 0.94 to theoretically enable daytime cooling, suffers from the same issue. Although silver as the back-reflector can achieve high solar reflectance, it is not stable and easily corrodeable in air when exposed to high level pollution (e.g. SO₂) and humidity (Yang and Zhang, 2020). Moreover, it is difficult to be directly put on emitters in a manner that yields high reflectance. Hence, non-silvered designs like polymers with comparable solar reflectance are more preferred.

It is well established that durability, cost and scalability are of great significance to promote real-world applications of daytime radiative cooling designs. By and large, nanophotonic designs with wavelength and subwavelength scales can have the unique ability to tailor spectral properties for selective thermal emittance, and by virtue of using inorganic materials, they are highly durable. Compared with 1-D planar photonic designs, 2-D and 3-D structures with higher degree of freedom (Liu et al., 2019b) can provide a higher emissivity in the atmospheric window (Santamouris and Feng, 2018). However, these designs are generally difficult to fabricate at scale due to the expensive, complex and stringent fabrication procedures involving, for instance, electron beam lithography or nanoimprint lithography (Zhao et al., 2019a). Therefore, photonic radiators are still largely limited to laboratory research and remain for further exploration. Paints as the most applicable radiative cooling design with the unique advantage of coating flexibility, are highly scalable and cost-effective, and can be made into near-ideal broadband coolers. For instance, the recent BaSO₄ or Al₂O₃-based

super-white paint coatings reported in (Mandal et al., 2020) yield the solar reflectance of ~ 0.98 and ~ 0.94, respectively, which are higher than or close to that of silvered cooling designs. However, their durability remains a challenge and they may use harmful chemicals. For porous paints, the effects of dust which may degrade the cooling performance should be carefully evaluated. Mechanical stability is also a potential concern for porous structure. Nanoparticles-embedded mixtures are less expensive by using the wet deposition and polymer melt fabrication methods, and thus easy for large-area applications to achieve radiative cooling. However, the challenges in controlling the size and distribution of the particles should be well addressed (Zeyghami et al., 2018). Polymers are inexpensive and manufacturable on a large scale. Polymer-based metamaterials are more likely to be widely applied in the future considering their overwhelming advantages over other nanophotonic materials regarding the manufacturability and cost (Santamouris and Feng, 2018). But they are facing the challenge of not being very durable under sunlight and easy to be aged. Moreover, polymer-based materials are basically susceptible to ultraviolet (UV) damages, which may degrade gradually after a long-term UV exposure (Council and Directory, 2019). The typical designs with adequate daytime radiative cooling capability are summarized in Table 2.

3.3. Applications of radiative cooling

3.3.1. Building cooling for energy savings

Building integrated passive radiative cooling can enormously contribute to low-energy buildings. In addition to the broad research on the direct integration with buildings in the form of radiative roof cooling which will be detailed in Section 4 considering preceding comprehensive studies, the indirect combinations of radiative cooling panels with various building systems have seen surging development which, based on adopted heat-exchange media, can be further divided into air-based, water-based and hybrid cooling systems (Lu et al., 2016; Zhao et al., 2019a). Air-based radiative cooling systems utilize air as the heat exchange medium (Mihalakakou et al., 1998; Parker, 2005; Parker and Sherwin, 2008). However, these types of cooling systems are generally small, restraining further applications. Water with a higher heating capacity can potentially increase the radiative cooling capacity. Basically, water-based cooling systems can be classified into open and closed systems (Zhao et al., 2019a). Roof water pond is a typical open system working by thermal radiation and evaporation to dissipate heat from indoor to outdoor environment (Ali, 2007; Kharrufa and Adil, 2008; Nahar et al., 2003; Sodha et al., 1981), while the required watertight roof structure limits its application in hot and arid regions (Lu et al., 2016). The closed water cooling system involves water as the heat carrier flowing through a closed pipe embedded in the flat-plate radiative system to provide cooled water. A pump is adopted to circulate the cooled water around the pipe and a water storage tank. The cooling energy preserved in liquid water can assist in achieving an energy-efficient building (Dimoudi and Androutsopoulos, 2006; Erell and Etzion, 1999; Hamza H. Ali et al., 1995; Meir et al., 2002; Saitoh and Fujino, 2001; Tevar et al., 2015). Nevertheless, in order to improve building energy efficiencies, hybrid systems are more desirable.

Technically, radiative cooling systems can have better performance by the integration with energy supply systems in buildings. The most promising way is to integrate radiative modules with air-conditioning systems to improve the overall working efficiency. Thanks to the latest realization of daytime radiative cooling material consisting of a birefringent polymer (Gentle and Smith, 2015), a non-evaporative water cooling panel was correspondingly demonstrated to cool water below the ambient as shown in Fig. 6 (Goldstein et al., 2017). Three days of the testing results with two cooling panels connected in series exhibited water temperature reductions of 3–5 °C corresponding to the cooling power about 40–70 W/m² at the water flow rate of 0.21 L/(min·m²). If the proposed cooling module is integrated with a condenser of an air-conditioning system, the system's efficiency can be significantly

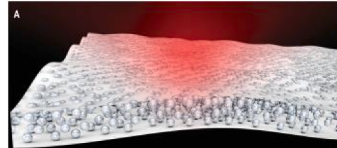
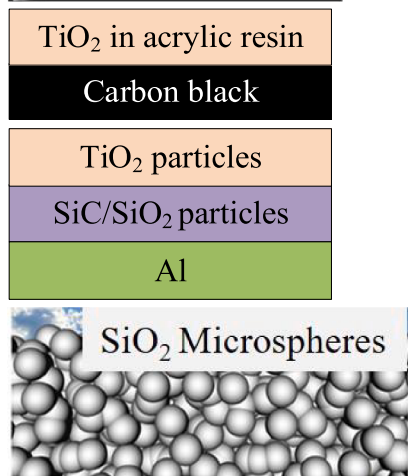
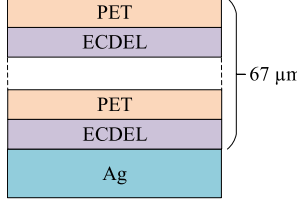
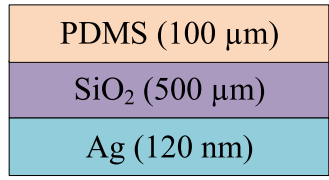
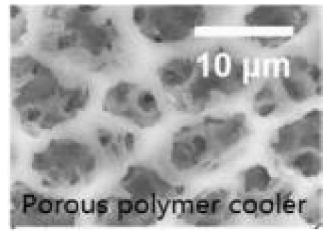
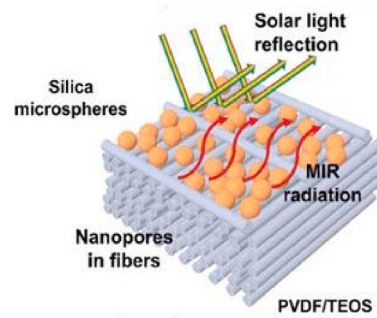
Table 2

Summary of typical designs with adequate daytime radiative cooling capability.

Materials/structures	Spectral property	Testing conditions	Cooling performance	Schematic diagram
Nanophotonic materials				
7 alternating layers of HfO ₂ and SiO ₂ atop a Ag substrate (Raman et al., 2014)	$\beta \sim 0.97; \epsilon \sim 0.5\text{--}0.8$ (8–13 μm) at 5° angle of incidence.	$G \sim 800\text{--}870 \text{ W/m}^2$ and $T_{\text{amb}} \sim 16\text{--}18^\circ \text{C}$ for ΔT test; $G \sim 860 \text{ W/m}^2$ and $T_{\text{amb}} \sim 21^\circ \text{C}$ for P_{net} test; Clear winter day at Stanford, California, USA (Experiment)	$\Delta T \sim 4.9 \pm 0.15^\circ \text{C}$; $P_{\text{net}} \sim 40.1 \pm 4.1 \text{ W/m}^2$	
Nano layers of Si ₃ N ₄ , amorphous Si and Al deposited atop a Si wafer (Chen et al., 2016)	$\epsilon_{\text{normal}} \sim 0.2\text{--}0.9$ (8–13 μm)	$G \sim 0\text{--}515 \text{ W/m}^2$; $T_{\text{amb}} \sim 0\text{--}18^\circ \text{C}$; A sun-shade mirror cone was used to block direct sunshine; Clear sky in winter at Stanford, California, USA (Experiment)	$\Delta T \sim 37.4^\circ \text{C}$ (average); $\Delta T \sim 42.2^\circ \text{C}$ (maximum)	
7 alternating layers of SiO ₂ and TiO ₂ with the top layer of Al ₂ O ₃ deposited on a Ag layer (Kecibas et al., 2017)	$\beta \sim 0.97; \epsilon \sim 0.75\text{--}0.77$ (averaged in 8–13 μm) at 15°–60° angles of incidence	Local solar irradiation and atmospheric transmittance in Istanbul, Turkey (Calculation)	$P_{\text{net}} \sim 100 \text{ W/m}^2$	
Nanostructure with 19 alternating layers of Al ₂ O ₃ and SiO ₂ on a Ag substrate (Wu et al., 2018)	$\beta \sim 0.95; \epsilon \sim 0.8\text{--}1$ (averaged in 8–13 μm) at angles of incidence less than 70°	$G \sim 964 \text{ W/m}^2$; $T_{\text{amb}} \sim 300 \text{ K}$ (Calculation)	$P_{\text{net}} \sim 122 \text{ W/m}^2$; $\Delta T \sim 47^\circ \text{C}$	
SiC and quartz layers for thermal emission; MgF ₂ and TiO ₂ layers on a Ag substrate for solar reflection (Rephaeli et al., 2013)	$\beta_{\text{normal}} \sim 0.965; \epsilon_{\text{normal}} \sim 0.1\text{--}0.95$ (8–13 μm)	$G \sim 964 \text{ W/m}^2$; $T_{\text{amb}} \sim 300 \text{ K}$ (Calculation)	$P_{\text{net}} \sim 105 \text{ W/m}^2$; $\Delta T \sim 40^\circ \text{C}$	
Conical metamaterial pillars comprising Al and Ge layers with an IR transmitting solar reflector atop a emitter (Hossain et al., 2015)	$\beta \sim 0.97; \epsilon \sim 0.90$ (8–13 μm) at 15°–30° angles of incidence	$G \sim 1000 \text{ W/m}^2$; $T_{\text{amb}} \sim 300 \text{ K}$; $h_{\text{nonrad}} \sim 6.9 \text{ W m}^{-2} \text{ K}^{-1}$ (Calculation)	$\Delta T \sim 9^\circ \text{C}$	
A metal-loaded dielectric resonator with phosphorous-doped n-type Si and Ag (Zou et al., 2017)	$\beta \sim 0.97; \epsilon \sim 0.8\text{--}0.95$ (8–13 μm) at 15°–30° angles of incidence	$G \sim 964 \text{ W/m}^2$; $T_{\text{amb}} \sim 300 \text{ K}$; $h_{\text{nonrad}} \sim 6.9 \text{ W m}^{-2} \text{ K}^{-1}$ (Calculation)	$P_{\text{net}} \sim 96 \text{ W/m}^2$; $\Delta T \sim 7.36^\circ \text{C}$	
Nano-and microparticle-based radiative materials				
A 50-mm-thick metamaterial film with 6% micro SiO ₂ spheres by	$\beta \sim 0.96; \epsilon \sim 0.93$ (averaged in 8–13 μm)	$G \sim 900 \text{ W/m}^2$; $T_{\text{amb}} \sim 17\text{--}35^\circ \text{C}$; Clear autumn days	$P_{\text{net}} \sim 93 \text{ W/m}^2$ at noontime; $P_{\text{net}} >$	

(continued on next page)

Table 2 (continued)

Materials/structures	Spectral property	Testing conditions	Cooling performance	Schematic diagram
volume backed with a Ag coating (Zhai et al., 2017)		in Cave Creek, Arizona, USA (Experiment)	110 W/m ² over continuous 72 h	
TiO ₂ in acrylic resin as top layer; Carbon black as bottom layer for thermal emission (Huang and TiO ₂ nanoparticles as top layer for solar reflection; SiO ₂ or SiC nanoparticles as bottom layer on an Al substrate for thermal emission (Bao et al., 2017)	$\beta \sim 0.91$; $\epsilon_{\text{normal}} \sim 0.95$ (8–13 μm); $\epsilon \geq 0.9$ (8–13 μm) at angles of incidence less than 60° $\beta \sim 0.907$; $\epsilon_{\text{hemispherical}} \sim 0.901$ (8–13 μm)	$G \sim 900 \text{ W/m}^2$; $T_{\text{amb}} \sim 300 \text{ K}$; PWV ~ 1 mm; $h_{\text{nonrad}} \sim 12 \text{ W m}^{-2} \text{ K}^{-1}$; (Calculation) Solar radiance of AM1.5; $T_{\text{amb}} \sim 30^\circ \text{C}$; $h_{\text{nonrad}} \sim 4 \text{ W m}^{-2} \text{ K}^{-1}$; PWV ~ 1.83 mm (Calculation)	$P_{\text{net}} \sim 100 \text{ W/m}^2$; $\Delta T \sim 6^\circ \text{C}$ $\Delta T \sim 5^\circ \text{C}$	
Low refractive index microspheres of SiO ₂ (Atiganyanun et al., 2018)	$\beta \sim 0.98$; $\epsilon_{\text{normal}} > 0.94$ (averaged in 8–13 μm)	$T_{\text{amb}} \sim 35.5\text{--}38.5^\circ \text{C}$; Clear sky under intense solar radiation in Albuquerque, New Mexico, USA (Experiment)	$\Delta T \sim 12^\circ \text{C}$	
Polymer-based radiative materials				
Polyethylene terephthalate (PET)/ECDEL polymer layers deposited on a Ag layer (Gentle and Smith, 2015)	$\beta \sim 0.97$ (from normal to 85° incidence); $\epsilon_{\text{hemispherical}} \sim 0.96$ (8–13 μm); $\epsilon_{\text{hemispherical}} \sim 0.63$ (3–23 μm)	$G \sim 1060 \text{ W/m}^2$; $T_{\text{amb}} \sim 27^\circ \text{C}$; Clear summer day with no convection shield in Sydney, Australia (Experiment)	$\Delta T \sim 2^\circ \text{C}$	
Polydimethylsiloxane (PDMS) film as top layer on a fused SiO ₂ wafer deposited on a Ag film (Kou et al., 2017)	$\beta \sim 0.9$; $\epsilon \sim 0.9\text{--}1.0$ (8–13 μm); ϵ near-unity over a broad bandwidth	$T_{\text{amb}} \sim 10.5\text{--}28.5^\circ \text{C}$; In Pasadena, California, USA (ΔT experiment); $T_{\text{amb}} \sim 300 \text{ K}$ under AM 1.5 solar irradiation (P_{net} calculation)	$\Delta T \sim 8.2^\circ \text{C}$; $P_{\text{net}} \sim 127 \text{ W/m}^2$	
Hierarchically porous polymer (P(VdF-HFP) _{HF}) ($\gtrsim 300 \mu\text{m}$) (Mandal et al., 2018b)	$\beta_{\text{hemispherical}} \sim 0.96 \pm 0.03$; $\epsilon_{\text{hemispherical}} \sim 0.97 \pm 0.02$ (8–13 μm)	$G \sim 890 \text{ W/m}^2$ (for testing ΔT) and 750 W/m^2 (for testing P_{net}); $T_{\text{amb}} \sim 26.5^\circ \text{C}$; PWV ~ 8 mm; Clear sky in Phoenix, Arizona, USA (Experiment)	$\Delta T \sim 6^\circ \text{C}$; $P_{\text{net}} \sim 96 \text{ W/m}^2$	
Polyvinylidene fluoride/tetraethoxysilane (PVDF/TEOS) fibers with nanopores inside and SiO ₂ microspheres (Wang et al., 2019)	$\beta \sim 0.97$; $\epsilon \sim 0.96$ (averaged in 8–13 μm) at 0°–60° angles of incidence	$G \sim 1000 \text{ W/m}^2$; $T_{\text{amb}} \sim 35^\circ \text{C}$; Humid day in Shanghai, China (Experiment)	$\Delta T \sim 3.5^\circ \text{C}$ (average); $\Delta T \sim 6^\circ \text{C}$ (maximum); $P_{\text{net}} \sim 61 \text{ W/m}^2$	
Polyethylene aerogel (PEA) as the top solar reflecting material combined with a selective emitter (Leroy et al., 2019)	$\beta \sim 0.922$; $\epsilon \sim 0.893$ (8–13 μm); $\gamma \sim 0.799$ (8–13 μm)	$G \sim 1123 \text{ W/m}^2$ and $T_{\text{amb}} \sim 6.4\text{--}25.8^\circ \text{C}$ for ΔT testing; $G \sim 936 \text{ W/m}^2$ and $T_{\text{amb}} \sim 26.2^\circ \text{C}$ for P_{net} testing; In October,	$\Delta T \sim 13^\circ \text{C}$ (average); $P_{\text{net}} \sim 96 \pm 9 \text{ W/m}^2$	

(continued on next page)

Table 2 (continued)

Materials/structures	Spectral property	Testing conditions	Cooling performance	Schematic diagram
Polyvinylidene fluoride (PVDF) or poly(methyl methacrylate) (PMMA) on a silver mirror layer (Aili et al., 2019)	$\beta_{\text{normal}} \sim 0.97$ (PVDF); $\beta_{\text{normal}} \sim 0.95$ (PMMA); $\epsilon_{\text{normal}} \sim 0.91$ (averaged in 8–13 μm) (PVDF); $\epsilon_{\text{normal}} \sim 0.89$ (averaged in 8–13 μm) (PMMA)	$G \sim 740\text{--}930 \text{ W/m}^2$; $T_{\text{amb}} \sim 10.5\text{--}33^\circ\text{C}$; In September, Boulder, Colorado, USA (Experiment)	$\Delta T \sim 6^\circ\text{C}$ (maximum) for PVDF; $\Delta T \sim 4^\circ\text{C}$ (maximum) for PMMA	
Polyethylene-based polymer filter with an emitter film below (Torgerson and Hellhake, 2020)	$\beta_{\text{hemispherical}} \sim 0.95$; $\epsilon \sim 0.85$; $\gamma \sim 0.75$ (8–13 μm)	$T_{\text{amb}} \sim 25\text{--}27^\circ\text{C}$; Relative humidity: 35%–45%; In Menlo Park, California, USA (Experiment)	$P_{\text{net}} \sim 110 \text{ W/m}^2$	
Polydimethylsiloxane (PDMS) as top thermal emitter with silicon dioxide on a silver layer (Jeong et al., 2020)	$\beta \sim 0.95$; $\epsilon \sim 0.98$ (8–13 μm)	$G \sim 1010 \text{ W/m}^2$; $T_{\text{amb}} \sim 23\text{--}35^\circ\text{C}$; Relative humidity ~ 87%; In Hong Kong, China (Experiment)	$\Delta T \sim 6.2^\circ\text{C}$	
Other radiative cooling designs				
Cellulose nanofibers-based wood structure (Li et al., 2019b)	$\beta \sim 0.96$ (incident angle of 8°); $\epsilon \geq 0.9$ (8–13 μm) at angle of incidence between ± 60°	$G \sim 0\text{--}730 \text{ W/m}^2$; $T_{\text{amb}} \sim 14\text{--}28^\circ\text{C}$; In Cave Creek, Arizona (Experiment)	$P_{\text{net}} \sim 16 \text{ W/m}^2$; $\Delta T \sim 4^\circ\text{C}$	
A porous membrane composed of anodic Al oxide (AAO) deposited on an Al substrate (Fu et al., 2019)	$\beta_{\text{normal}} \sim 0.94$; $\epsilon_{\text{normal}} \sim 0.98$ (8–13 μm) and ≥ 0.9 (8–20 μm)	$T_{\text{amb}} \sim 25\text{--}32^\circ\text{C}$; Relative humidity ~ 70%; Typical sunny day in Hangzhou, China (Experiment)	$\Delta T \sim 2.6^\circ\text{C}$	
SiO_2 mirror comprising SiO_2 bulk film atop a Ag film (Zhao et al., 2019b)	$\beta \sim 0.96$; $\epsilon \sim 0.79$ (averaged in 8–13 μm) and ~ 0.90 (averaged outside 8–13 μm)	$G \sim 680\text{--}965 \text{ W/m}^2$; $T_{\text{amb}} \sim 1.8\text{--}6.3^\circ\text{C}$; Clear day in Beijing, China (Experiment)	$\Delta T \sim 5.9^\circ\text{C}$	
Ultra-white glass on a Ag substrate for a specular surface; NaZnPO_4 particles on a polished Al substrate for a diffuse surface (Ao et al., 2019)	Specular surface: $\beta \sim 0.94$ and $\epsilon \sim 0.90$ (averaged in 3–25 mm); Diffuse surface: $\beta \sim 0.93$ and $\epsilon \sim 0.7$ (averaged in 3–25 mm) at the incidence angle of 5°	$G \sim 430 \text{ W/m}^2$; $T_{\text{amb}} \sim -1.5\text{--}11.5^\circ\text{C}$; Relative humidity: 20–85%; Wind speed: 0–4 m/s; In Being, China (Experiment)	Specular surface: $\Delta T \sim 2.5^\circ\text{C}$; Diffuse surface: $\Delta T \sim 1.5^\circ\text{C}$	

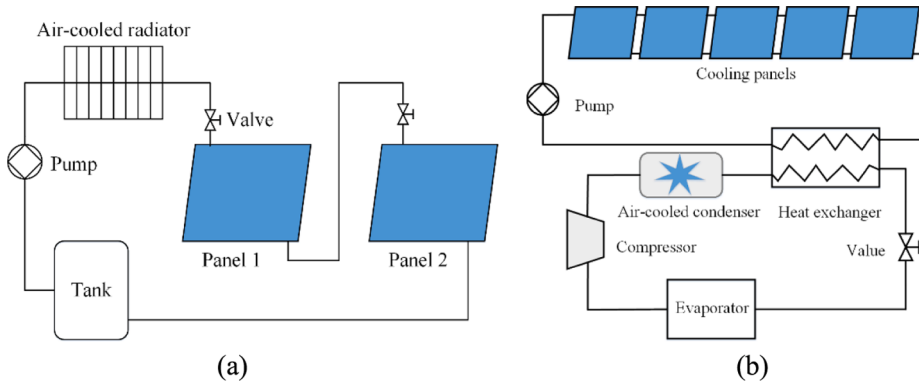


Fig. 6. The non-evaporative water cooling panel. (a) Piping configuration with two cooling panels connected in series. (b) Radiative cooling connected with a condenser (Goldstein et al., 2017).

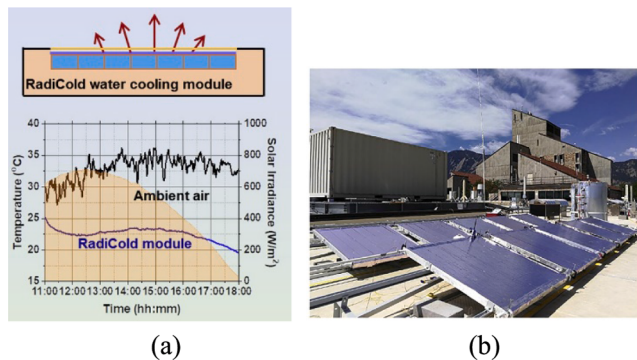


Fig. 7. Sub-ambient radiative cooling panels. (a) Schematic of the cooling module and test results. (b) Photograph of the modules (Zhao et al., 2019c).

improved compared to a standard air-cooled chiller. A two-story building simulation demonstrated the reduced electricity usage by 21% during summertime.

Similarly, but more promisingly, a radiative cooling system which utilized the glass-polymer hybrid metamaterial was proposed to provide cooling water as shown in Fig. 7. Sub-ambient cooled water of 10.6 °C could be achieved by the system at noon under direct sunlight (Zhao et al., 2019c). Moreover, a kilowatt-scale radiative cooling system was built with the maximum nocturnal cooling power of 1296 W. The system can realize two operating strategies by controlling intermittent flow to produce water under sub-ambient temperatures and continuous flow to achieve maximum cooling energy. The cooled water can be directly utilized for condenser cooling. However, considering the limited cooling demands at night, an operating mode combining the daytime condenser cooling and nighttime storage was further developed, which was applied to a commercial office building under three regions in the U. S. (Phoenix, Houston, and Miami). The results demonstrated the energy saving rates of 64%-82% in winter and 2%-45% in summer.

Regarding the pumping energy of lifting water up to the cooling panels for the above two sub-ambient cooling systems in high-rise buildings, water is pumped from the ground tank to the roof water storage tank before being transported into the radiative cooling panel for conducting heat exchange. The cooled water from the radiative coolers will be further utilized to cool condensers of air-conditioning systems in each floor through downfeed via gravity. Hence, the pumping power can be expressed as (Cheng, 2002; Cheung et al., 2013)

$$E_{pump} = \frac{\rho g H Q}{3600 \eta_c} \quad (8)$$

where E_{pump} is the pumping power of a lift pump, W; ρ is the water density, 1000 kg/m³; g is the acceleration of gravity, 9.8 N/kg; H is the

height of water being lifted from the ground pump to the cooling panels in the building rooftop, m; Q is the volumetric water flow rate of pumping system, m³/h; η_c is the overall transmission efficiency which can be calculated by

$$\eta_c = \eta_p \eta_m \eta_e \quad (9)$$

where η_p is the pump efficiency; η_m is the mechanical transmission efficiency; η_e is the electric motor efficiency. For simplicity, constant efficiencies are assumed (Cheung et al., 2013) with $\eta_p = 0.65$, $\eta_m = 0.9$, $\eta_e = 0.9$, and thus $\eta_c = 0.5265$. Actually many residential buildings in the densely populated city like Hong Kong are over 40 storeys or over 100 m with the average height estimated to be 25.8 storeys (Cheung et al., 2013). Considering the roof tank usually has a minimum height of 3–7 m above the rooftop surface (Cheng, 2002), and given a story height of 3 m, H is estimated to be 80.4 m (=3 × 25.8 + 3). For the reported water flow rate of 26.5 L/(h·m²) and radiative cooling surface area of 13.5 m² in (Zhao et al., 2019c), based on Equations (8) and (9), the calculated pumping power is 148.7 W, which is below the noontime and nighttime cooling powers of 607 W and 1296 W, respectively, indicating the potential profits from using the radiative cooler in high-rise buildings. More broadly, if a larger roof area of 100 m² is assumed as the radiative cooling surface, the necessary pumping powers for radiative cooling modules in (Zhao et al., 2019c) and (Goldstein et al., 2017) are 1104.6 and 498.8 W, respectively. Whilst according to the recorded cooling power rates of 45–96 W/m² in (Zhao et al., 2019c) and 40–70 W/m² in (Goldstein et al., 2017), the obtained total cooling powers will be 4500–9600 W and 4000–7000 W, respectively, which are much higher than the required pumping powers. Thereby, radiative cooling technology to cool pumped water is technically and economically feasible

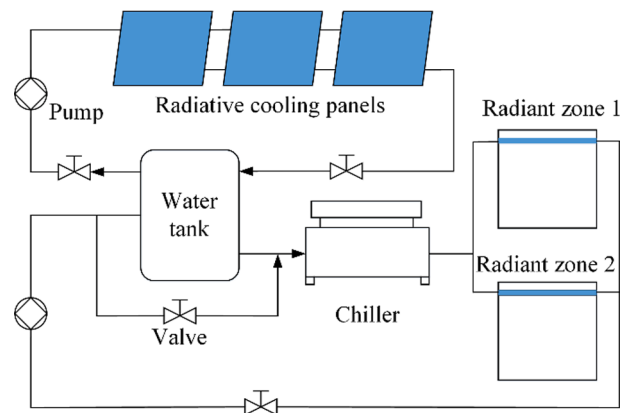


Fig. 8. Schematic of the photonic-based radiative cooling system (Wang et al., 2018).

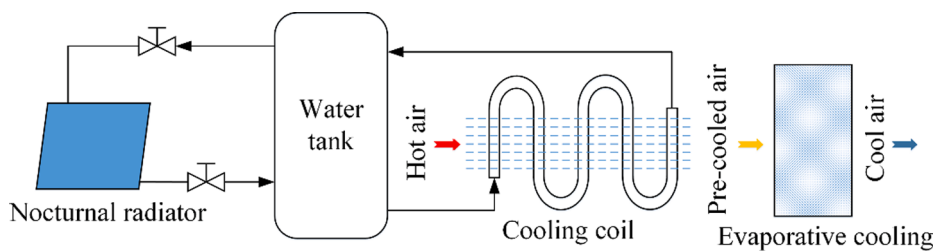


Fig. 9. Integration of nocturnal radiator with direct evaporative cooling system (Heidarinejad et al., 2010).

for high-rise buildings.

Based on the 1-D planar photonic material in (Raman et al., 2014), Wang et al. (2018) developed a photonic-based radiative cooling system and evaluated the energy saving performance for a medium-sized office building (5000 m^2) with the adopted radiator accounting for 60% of the roof area as shown in Fig. 8. The proposed system comprised two hydronic loops: a space-cooling loop and a radiative water cooling loop, both of which were connected via a water storage tank which was serially connected with an air-cooled chiller to provide cooled water to radiant slab surfaces. The proposed photonic cooling system could numerically save electricity consumption from 45% to 68% compared to VAV systems, while the saving rates were 9%–23% compared to a cool roof-based nocturnal radiative cooling system.

Since heat pumps are significant building power supply systems, radiative cooling modules could be a good supplement as heat rejectors to improve the overall system efficiency. Man et al. (2011) integrated a nocturnal cooling radiator with a ground coupled heat pump (GCHP) system to address the issue that heat rejected from the building into the ground results in the degradation of overall system performances. The system operations for a typical building in Hong Kong were analytically modeled, which exhibited the total cost saving rate of 10.22% for a 10-year operation relative to a traditional GCHP system. Furthermore, the combination of nocturnal radiators with evaporative cooling systems to strengthen pre-cooling effects can augment systematic cooling efficiencies as shown in Fig. 9 (Heidarinejad et al., 2010). During the nighttime, the cooled water produced by the radiator is transported to the water tank, while during the daytime the chilled water would flow through the cooling coil unit to exchange cooling energy with hot outdoor air for a preliminary cooling before going through a direct evaporative cooling procedure. The hybrid system overcame the shortcoming of energy supply shortage by a stand-alone evaporative system, which could obtain the overall efficiency over 100%. The radiative module can also be combined with indirect evaporative cooling system to achieve better energy-efficient cooling effects (Farmahini-Farahani and Heidarinejad, 2012; Farmahini Farahani et al., 2010).

Considering the low-density properties of the power generated from radiative cooling modules, phase change materials (PCM) serving as a thermal storage medium can be potentially combined with radiative coolers for energy storage to ensure cooling power supply. In some passive and low-energy buildings, PCM ceilings cooled by cold water can

provide cooling energy accounting for 11% of total cooling loads (Eicker and Dalibard, 2011). Therefore, Zhang and Niu (2012) proposed a combination of a microencapsulated PCM (MPCM) slurry with a nocturnal radiative cooler as demonstrated in Fig. 10. During the nighttime, the produced cooling power was stored in the MPCM slurry, while during the daytime the cooling energy was transferred to the pipe water to cool buildings. Energy saving rate over 77% was numerically achieved for a low-rise building under dry weather conditions. Lei et al. (2017) further studied the cool colored coating integrated with MPCM as exterior surfaces for building cooling. The dual effects by cool paints for the solar reflection and the PCM coating for remaining heat absorption work complementarily to achieve optimal cooling results. The PCM integrated with cool roofs to reduce heating penalties during winter seasons was also investigated (Chung and Park, 2016).

By and large, the cooling power produced from passive radiative panels can be integrated with buildings in a variety of ways to improve energy efficiency and achieve energy savings. The cooled water can be either utilized to cool condensers of air conditioning systems to reduce electricity consumption or transported directly into the radiant ceiling slabs through hydronic loops for indoor space cooling and thermal comfort improvement. More broadly, the concept of radiative cooling can be further combined with various building power supply systems to enhance systematic energy performance. For instance, radiative cooling modules can work in tandem with ground coupled heat pumps as heat rejectors to enhance overall system efficiency. The chilled water combined with cooling coils as a preliminary cooling process can prominently overcome the drawback of energy shortage from a stand-alone evaporative cooling system. With respect to the thermal storage, the radiative cooling power can also be stored in phase change materials to ensure a continuous and adequate cooling power supply for buildings.

3.3.2. Solar cell cooling for efficiency enhancement

Solar power is a significant renewable energy to reduce consumption on fossil fuels and facilitate the realization of a pollution-free society. However, the photovoltaic conversion efficiency is still a bottleneck facing the industry due to a small portion of absorbed solar power being converted to electricity while remaining energy being wasted as heat inducing the temperature increase of solar panels. Basically, current

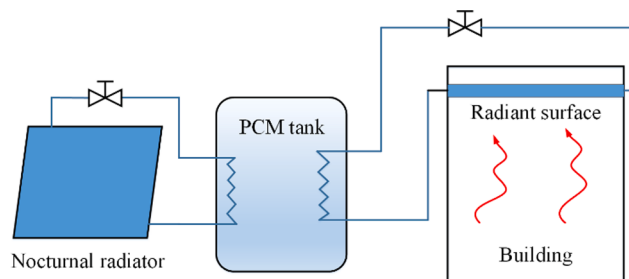


Fig. 10. Schematic of nocturnal radiative cooling integrated with PCM for thermal storage (Zhang and Niu, 2012).

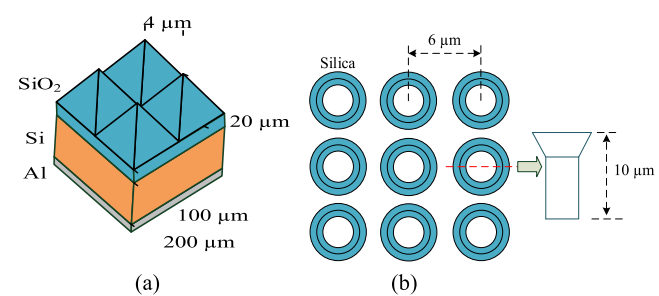


Fig. 11. Schematic of approaches for solar cell radiative cooling. (a) Square lattice of SiO_2 pyramids atop a uniform SiO_2 layer (Zhu et al., 2014). (b) SiO_2 square-lattice photonic crystal by etching 10- μm deep air holes into a fused SiO_2 wafer (Zhu et al., 2015).

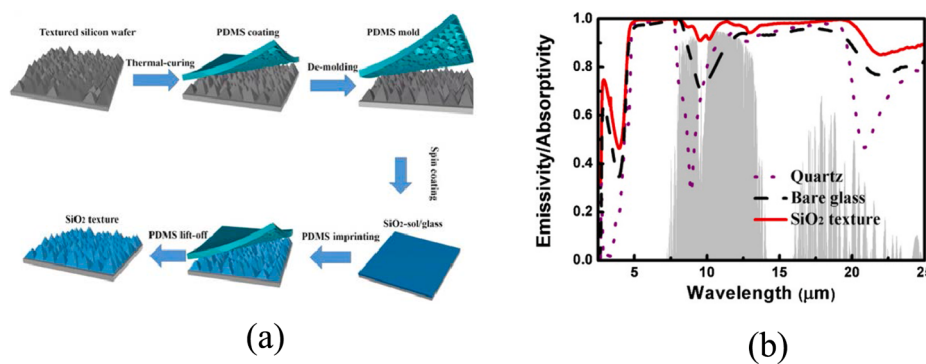


Fig. 12. Schematic of the SiO₂ based sol-gel imprinted texture glass. (a) Fabrication process of the texture glass. (b) Comparison of spectral emittance (Lu et al., 2017).

commercial solar cells have the module efficiency less than 20%, indicating >80% of the absorbed solar radiation being dissipated as heat. Operating at an increased temperature exerts an adverse effect on the PV modules' performance considering a reduced PV power conversion efficiency under a higher temperature (Zhao et al., 2020b). For instance, an increase of 1 °C in PV panels reduces conversion efficiencies by 0.4–0.5% for crystalline silicon cells (Zhao et al., 2019a). Another issue is the increased aging rates of solar modules under an elevated temperature (Sun et al., 2017b). Therefore, seeking a highly efficient and cost-effective way to reduce solar cell operating temperatures is significant to fulfill an efficient and resilient solar PV based renewable system.

The intrinsic cooling capacity of current solar cells is quite limited due to the low infrared emissivity of bare silicon. The basic idea to achieve radiative cooling of solar cells is by applying a surface coating which is transparent to solar radiation while highly emissive in mid-infrared spectral wavelengths on top of solar cells, the development of which has made progress. For instance, Zhu et al. (2014) developed a cooling material composed of silica pyramids with 2-D square lattices as the thermal emitter atop a silica substrate, which showed almost transparency to incident solar radiation and great improvement of IR emissivity in comparison to the bare silicon (Fig. 11(a)). The analytical temperature reduction of 17.6 K under the solar radiation of 800 W/m² resulted in the absolute efficiency improvement of 1.6%. Following this structure, Zhu et al. (2015) proposed another 2-D silica material composed of a square-lattice photonic crystal structure (Fig. 11(b)). When placed on a silicon absorber under sunlight, the structure reduced the temperature by up to 13 °C. Furthermore, an improved SiO₂-based sol-gel imprinted texture glass was fabricated to enhance light and thermal management of solar cells by simultaneously increasing the light trapping and radiative cooling capacity (Lu et al., 2017). During the fabrication process, a PDMS coating was used as an intermediate structure mold to shape the cooling material (Fig. 12). Owing to phonon-polariton resonances of silica textures, the emittance at the middle infrared wavelengths was enhanced >96% within the atmospheric transparency window and the solar transmittance over 94% was simultaneously achieved. By applying the material to a crystalline silicon PV module, the relative conversion efficiency was enhanced by 3.13%.

More promisingly, considering the high absorption of current solar cells in sub-band gap (1.1–1.8 μm) and UV wavelength band (0.3–0.375 μm) which results in excessively detrimental heat generation, undermining working efficiency and accelerating the degradation process, Li et al. (2017) developed a multilayer dielectric stack comprising Al₂O₃, SiN, TiO₂ and SiO₂ atop an encapsulated solar panel. The material has the ability to restrain the absorption of UV and sub-band gap while preserve the spectrum absorption from 0.375–1.1 μm. The surface temperature could be reduced by 6.2–15.4 °C with the improved solar cell efficiency of 1.52%. Moreover, the new structure enables to overcome the drawback of a large dip near 9 μm caused by the phonon-

polariton excitation of the bulk silica, thus maximizing solar cell cooling performance. The surface temperature of solar cells can be lowered by 5.7 °C to improve the absolute efficiency by 0.56% for silicon solar cells with the temperature coefficient of 0.45% (Skoplaki and Palyvos, 2009). Likewise, Munday and Safi (2016) exhibited a photonic material above a GaAs solar cell to improve its thermal emission for radiative cooling, which achieved a cooling temperature of 18 °C lower than a traditional solar cell (Safi and Munday, 2015). A sub-band gap optical filter was implemented to eliminate the parasitic absorption, and the solar cell surface was modified to enhance thermal emission for radiative cooling of CIGS solar cells (Sun et al., 2017a). Based on the optics-based approach, one-sun terrestrial solar panels could be cooled up to 10 °C. Specifically, the effects of radiative cooling are more prominent under high temperature scenarios, like concentrating PV (CPV) systems (Nishioka et al., 2013). The low-iron soda-lime glass was utilized to realize radiative cooling in these systems (Sun et al., 2017c; Zhou et al., 2016). Although radiative cooling applications on solar cells were extensively reported, some doubts were cast on the practical effectiveness which may be counteracted at moderate wind speeds (Gentle and Smith, 2016). Additionally, the radiative cooling modules can be further integrated with hybrid solar energy utilization systems like photovoltaic-thermal (PVT) collectors and conversion systems to strengthen cooling capacities (Eicker and Dalibard, 2011; Hu et al., 2016; Hu et al., 2018; Hu et al., 2017; Zhao et al., 2020a; Zhao et al., 2017; Zhao et al., 2018).

To sum up, passive radiative cooling integrated with solar cell panels is potentially an efficient and cost-effective way to improve photovoltaic conversion efficiency. Basically, the surface spectral properties above solar cells should be tailored with high solar transmission to guarantee the inherent electricity generation and strong infrared emittance to dissipate heat for temperature reductions. More remarkably, the

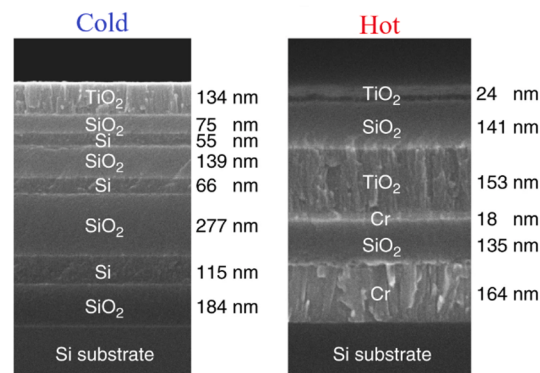


Fig. 13. Color preserving material. Cold structure: 7 layers of Si and SiO₂ with TiO₂ as the top layer; hot structure: 3 bottom metal-insulator-metal layers and 3 top dielectric layers (Li et al., 2018).

excessive heat produced by the solar absorption in the sub-band gap and UV wavelength of numerous solar cells can be substantially restrained to enlarge the temperature reduction and bring more considerable efficiency enhancement.

3.3.3. Other advanced exploitations

(1) Color preserving radiative cooling designs

In addition to the abovementioned applications, radiative cooling can also be extended to other advanced exploitations. Cooling a surface while preserving its original color is preferred for occasions where glare is not expected, which can be fulfilled by maintaining the original solar reflectance while increasing the infrared emittance. For instance, blending reflective and transparent pigments to tailor infrared properties was reported to produce such a single functional coating (Brady and Wake, 1992). Levinson et al. (2007) described methods for creating solar-reflective nonwhite surfaces, which were applied to a variety of residential roofing materials. Coloring a topcoat with pigments (e.g. chrome or nickel titanate yellow) to strongly backscatter near-infrared (NIR) (0.7–2.5 μm) radiation can maximize reflectance in the NIR spectrum. For instance, coated steel and glazed clay-tile roofing products can obtain the NIR reflectance of 0.5 and 0.75, respectively. Furthermore, a new process for coating concrete tiles and asphalt shingles to increase both the solar reflectance and factory-line throughput was demonstrated by using a two-layer spray coating (Levinson et al., 2010), where the titanium dioxide rutile white basecoat was adopted as the first layer to increase solar reflectance, and a cool color topcoat was the second layer. Both layers dry within seconds to potentially enlarge factory output. Zhu et al. (2013) modified the structure of silicon nanowires by using an array of optically transparent and thermally emissive material of quartz bars. The new structure could analytically reduce the material temperature by 31.4 K. More potentially, Li et al. (2018) utilized TiO_2 , SiO_2 , Si based alternating layers to fabricate a cold and a hot photonic structures while preserve the same pink color (Fig. 13). The experimental results demonstrated that the hot photonic structure could reach over 88 °C whilst the cold one stayed below 40 °C, and both structures are over 20 °C either hotter or cooler than a commercial paint with a comparable color. Recently, Chen et al. (2020) proposed a novel paintable bilayer coating which is composed of a thin, visible-absorptive layer atop a nonabsorptive, solar-scattering underlayer to satisfy the need for color preserving whilst simultaneously achieve radiative cooling. Compared with a conventional same colored monolayer paint, the porous P(Vdf-HFP) in (Zhai et al., 2017) as a solar-scattering underlayer improved the reflectance of near-to-short infrared light by 0.51. The cooling performance of 15.6 °C lower temperature was achieved by utilizing the black porous P(Vdf-HFP)-based bilayer than that of the monolayer black coating under the solar intensity of $\sim 1025 \text{ W}\cdot\text{m}^{-2}$.

(2) Adaptive radiative cooling designs with tuneable optical property

Currently, most of the existing radiative cooling systems are static with fixed optical properties of solar reflectance and thermal emittance. However, as external temperature varies daily and seasonally, cooling effects are not always desired especially during the nighttime in winter. Therefore, adaptive radiative cooling designs with tuneable optical properties to enable cooling in hot days while disable cooling under cold conditions are highly desirable. In accordance with this concept, Ono et al. (2018) proposed a self-adaptive radiative cooling system by utilizing the phase change material of vanadium dioxides (VO_2) incorporated with a planar photonic multilayer system and a spectrally selective filter to adaptively switch radiative cooling according to the ambient temperature. Once the transition temperature of VO_2 is reached, VO_2 is in the metallic state with minimum solar absorption and strong selective emissivity from 8 to 13 μm to automatically turn on the system's radiative cooling functionality. While if the temperature drops below transition temperature with VO_2 changing to low thermal emissive insulating state, the cooling process will be turned off. Regarding this application, the control and realization of appropriate phase transition

temperature is crucial for the adaptive performance. More phase change materials for switchable optical properties were discovered in (Abdolahramezani et al., 2020; Kim et al., 2019; Qu et al., 2018; Taylor et al., 2017). Besides, electrochromic materials were also reported with the ability to adjust the optical properties for thermoregulation (Chandrasekhar et al., 2014; Mandal et al., 2018a). $\text{Li}_4\text{Ti}_5\text{O}_{12}$ with visible-to-infrared electrochromic properties was developed with large tunabilities of 0.74, 0.68, and 0.30 for solar reflectance, mid-wave and long-wave infrared emittance, respectively (Mandal et al., 2018a).

More recently, Mandal et al. (2019) proposed simple and cost-effective porous polymer coatings (PPCs) of which the switchable optical transmittance can be regulated through wetting operations with common liquids. The optical switching of a porous P(Vdf-HFP) was demonstrated, whose pore sizes could be largely diminished upon wetting to reduce the scattering efficiencies by 10^1 - 10^3 to turn transparent, whilst the process is reversible to dry state with air in the pores for the high solar reflection. The P(Vdf-HFP)-based PPCs could attain solar and visible transmittance changes of up to 0.74 and 0.80 for the control of daylight and heat in buildings. Moreover, the polytetrafluoroethylene PPCs as switchable roofs have been experimentally demonstrated with sub-ambient passive daytime radiative cooling of 3.3 °C under the dry state and above-ambient solar heating of 21.4 °C under the wet state. The polyethylene PPCs exhibit the switchable thermal infrared transmittance by 0.64. The changes in solar and thermal transmittance can be used for seasonal or diurnal thermoregulation in buildings. Another fluidic designs with tuneable solar transmittance and thermal emittance have also been demonstrated in (Syurik et al., 2018) where the phase separation method was used to manufacture scattering porous polymer films constituted by polymethyl methacrylate (PMMA) with the broadband reflectivity of $\sim 75\%$ under 4 μm thickness. Upon wetting using liquids like water or ethanol, the film is index-matched to change from white to transparent allowing for tunable transmittance-based applications.

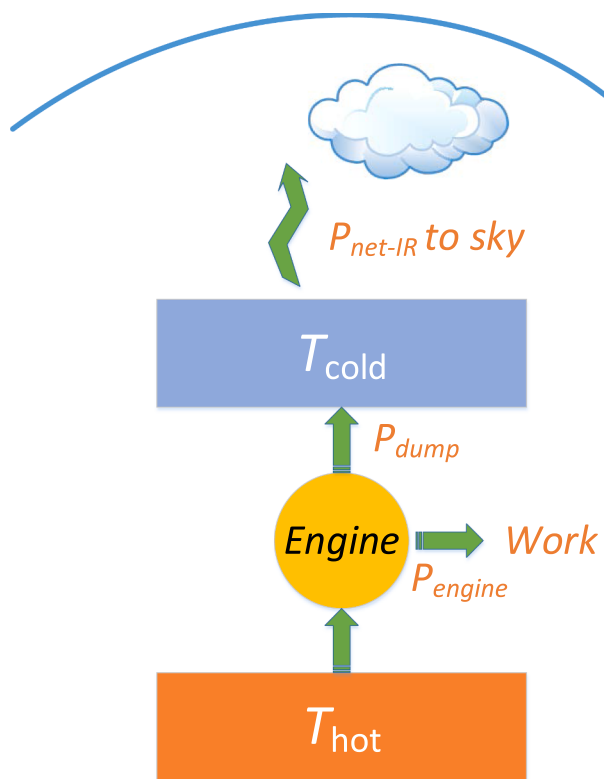


Fig. 14. Schematic of an emissive energy harvester via radiative cooling with energy flowing from a heat sink (T_{hot}) to a cold reservoir (T_{cold}) through an engine, converting a portion of heat into work.

(3) Emissive energy harvester

The earth continuously emits power of 10^{17} W to outer space. If properly utilized, the energy can satisfy the basic needs of human beings. Radiative cooling can be potentially designed as emissive energy harvesters (EEHs) to harness a portion of the heating energy transmitted from the heat sink to cold reservoir (Byrnes et al., 2014; Fernández, 2020; Strandberg, 2015; Zeyghami et al., 2017). As shown in Fig. 14, based on Carnot's law with the steady-state heat flow, the output power from the engine is (Byrnes et al., 2014)

$$P_{\text{engine}} \leq P_{\text{net}} \times \left(\frac{T_{\text{hot}}}{T_{\text{cold}}} - 1 \right) \quad (10)$$

where T_{hot} , T_{cold} , and P_{net} are the heat sink temperature, cold reservoir temperature and net radiative cooling power. As illustrated in Fig. 3 in Section 2.3.1, a higher cold reservoir temperature T_{cold} corresponds to a larger radiative cooling power P_{net} , while Equation (10) indicates more engine power P_{engine} can be achieved under both a higher P_{net} and a lower T_{cold} . Thus, there exists an optimal temperature of cold reservoir T_{cold} to maximize output engine power under a fixed T_{hot} . If the ambient is used as the heat sink, the optimized maximum output engine power is about 2.7 W/m^2 (Liu et al., 2019b), which, however, could reach up to 300 W/m^2 with the heat sink temperature of 500 K (Sun et al., 2017b). Hence, a heat sink with a higher temperature (e.g. industrial waste heat or heat from solar absorbing materials) induces more significant output powers. Such high temperature of T_{hot} ensures an optimal T_{cold} above ambient temperature, which can be realized by numerous materials with the broadband emissivity to fulfill emissive energy harvesting applications. EEHs can be basically divided into thermal EEHs which are analogous to solar thermal powers and optoelectronic EEHs that are parallel to photovoltaic power utilizations to fulfill energy harvesting. Specifically, semiconductors, such as rectifying antennas (Knight et al., 2011), can be used to implement EEHs. However, the dominant auger recombination (Bedford et al., 2011) may impede such practical implementation. Nevertheless, considering the enormous thermal radiation from the earth to universe, this energy harvesting approach via incessant radiative cooling will be an advanced and promising technology for further investigation.

(4) Radiative cooling-assisted thermoelectric application

Conceptually, the existence of temperature difference with one side as the hot source and another as the cold sink can be thermodynamically converted to electricity. Due to the fact that the outer space is a ubiquitous cold sink, accessing the coldness of space by radiative sky cooling can achieve satisfactory sub-ambient temperatures. Thereby, utilizing the ambient air as the heat source and outer space as the cold sink enables to obtain continuous temperature differences for electricity generation. To fulfil the purpose of energy conversion, a thermoelectric generator (TEG) working on the basis of Seebeck effect turns out to be a

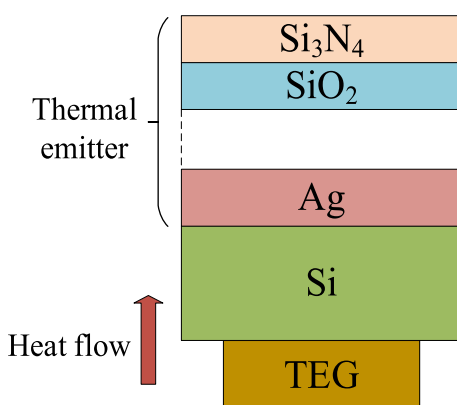


Fig. 15. Planar structure composed of alternating SiO₂ and Si₃N₄ coated on a silver layer for thermoelectric power generation (Mu et al., 2019).

tractable and direct option. To eliminate the dependence on active input of heat when using thermoelectrics for night-time power generation, Raman et al. (2019) experimentally demonstrated a simple, low-cost and entirely passive way to generate electricity by combining radiative sky cooling with a thermoelectric module, where the cold side was coupled to a black thermal emitter ($\epsilon \sim 0.95$) directly facing the sky and the hot side was placed under the ambient for natural convection. The demonstrated power rate of 25 mW/m^2 was able to power a light emitting diode operating at about 10% of its maximum brightness. Additional reports regarding the radiative cooling-assisted thermoelectric power generation were also demonstrated. For instance, recently a new planar structure composed of alternating SiO₂ and Si₃N₄ coated on a silver layer was developed (Mu et al., 2019) (Fig. 15). The optimal periodicity of the SiO₂/Si₃N₄ alternating layers was testified with the maximum thermal emittance of 80.8%. A 24 h test showed the nighttime temperature drop reached up to 4 K. A sub-micro thermoelectric generation device was placed on the other side to utilize the cooling power as a self-sustained power system, which obtained the maximum output voltage of 0.5 mV. A radiative cooler consisting of a glass substrate and an aluminum thin film combined with a thermoelectric module could continuously generate positive voltages throughout a day (Ishii et al., 2020). Moreover, when compared to using an untreated aluminum heat sink, the thermoelectric output with the improvement of the radiative cooling capacity has been enhanced by 55%-70% by using 30–40 μm thick nanoporous alumina grown on aluminum surfaces (Zhan et al., 2019). In the same vein, the power generated from the TEG with radiative cooling heat sink modules turns out to be 32% higher than that with aluminum heat sink module in an arid city (Liu et al., 2020).

Another prominent application would be to integrate radiative sky cooling with thermoelectric cooling (TEC) so as to improve system COP. Considering most of the current building-integrated thermoelectric cooling systems with COPs less than 1 (Irshad et al., 2015), Zhao et al. (2020d) studied the performance of a radiative sky cooling-assisted thermoelectric cooling system applied in buildings. The hot side of the TEC subsystem was cooled by the cooling power from the radiative cooler based on the thin film metamaterial in (Zhai et al., 2017). Through a case study for a residential building, the annual system COP could be enhanced to 1.87.

4. Radiative roof cooling development

Radiative cooling has been directly applied to building roof structures in the form of cool roof for decades with considerable preceding studies. Cool roof which is a kind of radiative roof surface with a high solar reflectance and thermal emittance is the most direct and mature example of passive radiative cooling integrated with buildings (Lu et al., 2016; Zhao et al., 2019d). Such practice which though cannot achieve sub-ambient cooling still exhibits large cooling potential for roof temperature reductions and building energy savings. Hence, a thorough review on current cool roof studies will apparently contribute to the future development of radiative roof cooling by integrating recent daytime cooling material designs. Actually, the “cool roof scheme” has been initiated in America which set up standards for roof products involving the parameters of solar reflectance and thermal emittance. The authorities of ENERGY STAR (ENERGY STAR, Certified Roof

Table 3

Examples of building codes for cool roof qualifying criteria (Akbari and Levinson, 2008).

The U.S. Code	Building types	Criteria
ASHRAE 90.1	Commercial and high-rise residential buildings	SR > 0.55 and TE > 0.75, or SRI > 64
ASHRAE 90.2	Low-rise residential buildings	SR > 0.65 and TE > 0.75, or SRI > 75
California Title	Buildings with low-sloped roofs	Aged SR > 0.55 and TE > 0.75, or SRI > 64

Table 4
Typical roof materials (Council and Directory, 2019; Testa and Krarti, 2017).

Product	Solar reflectance	Thermal emittance	SRI
Smooth Bitumen	0.06	0.86	-1
Generic Black Shingle	0.05	0.91	1
Light Gravel	0.34	0.90	37
Aluminum	0.61	0.25	56
White Coating on Shingle	0.71	0.91	87
Alpha 8 505 Coating	0.84	0.92	106
ArmorFlex White Liquid Roof Membrane AP-585	0.90	0.90	114
R-Mer Coat 1531 Coating	0.93	0.90	119

Products, 2019) and Cool Roof Rating Council (Council and Directory, 2019) both operate voluntary labeling programs and list the certified or rated roof products to provide guidance for customers. Moreover, in order to facilitate the cool roof scheme and give clients more information about the benefits from applying cool roof products, the U.S. Department of Energy introduced a "Cool Roof Calculator" (Laboratory, 2020) to help predict energy savings for flat non-black roof surfaces. Technically, there are several metrics to evaluate the cool roof performance, namely the initial and 3-year aged solar reflectance (SR), thermal emittance (TE) or solar reflectance index (SRI), which are usually specified in cool roof products. The SRI is a coolness indicator that incorporates both solar reflectance and thermal emittance to signify roof temperatures under sunlight. The index indicates how hot a surface would be when compared to a standard black surface ($SRI = 0$, SR = 0.05, TE = 0.90) and a white surface ($SRI = 100$, SR = 0.8, TE = 0.9) as defined in Equation (11):

$$SRI = \frac{(T_{black} - T)}{(T_{black} - T_{white})} \times 100 \quad (11)$$

here, T_{black} and T_{white} are the standard black and white surface temperatures, and T is the investigated surface temperature. Actually, SRI can be below 0 for extremely hot objects like solar collectors or over 100 for super cool surfaces. A SRI calculator (Laboratory and Calculator, 2020) was developed to help rapidly evaluate the roof coolness. Many building codes were proposed accordingly in the U.S. to define cool roof criteria for different building types by the three metrics as summarized in Table 3, and typical roof materials are listed in Table 4.

Other than pure white cool roof surfaces, from the perspective of esthetics the roof surface which keeps the originally designed color while still maintains cooler than the traditional roof will be more

desirable considering the glaringness alleviation. To this end, the "Cool Colors Project" was initiated by California Energy Commission (Heat Island Group, 2020) aiming to develop cool colored roof products which only reflect the "near-infrared" range of solar spectrum so as to preserve roof colors. Synnefa et al. (2007b) investigated a bunch of cool colored coatings which have the same colors to conventional pigmented coatings but a higher solar reflectance, and found that lower surface temperatures for cool colored coatings could be achieved with the maximum temperature difference of 10.2 °C. Additionally, some rebate programs were initiated to promote the cool roof scheme (Akbari and Levinson, 2008). Generally, cool roof implementations were constrained to bulk materials without adequate daytime cooling capability. The integration of latest daytime radiative cooling materials will tremendously contribute to its development.

4.1. Cool roof-based heat transfer model

4.1.1. Heat flux through roof structure

Heat gains or losses through roof structures will essentially affect the indoor thermal comfort and energy consumption in buildings. The intensity of heat flux is subject to the radiative and convective heat

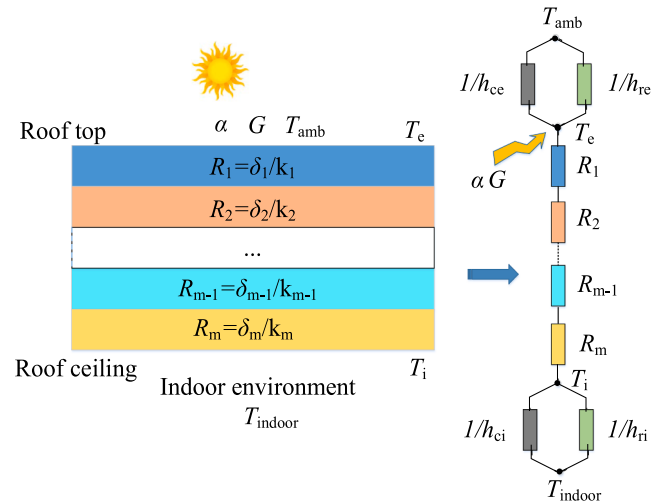


Fig. 17. Resistance model for heat transfer through a multilayered roof structure.

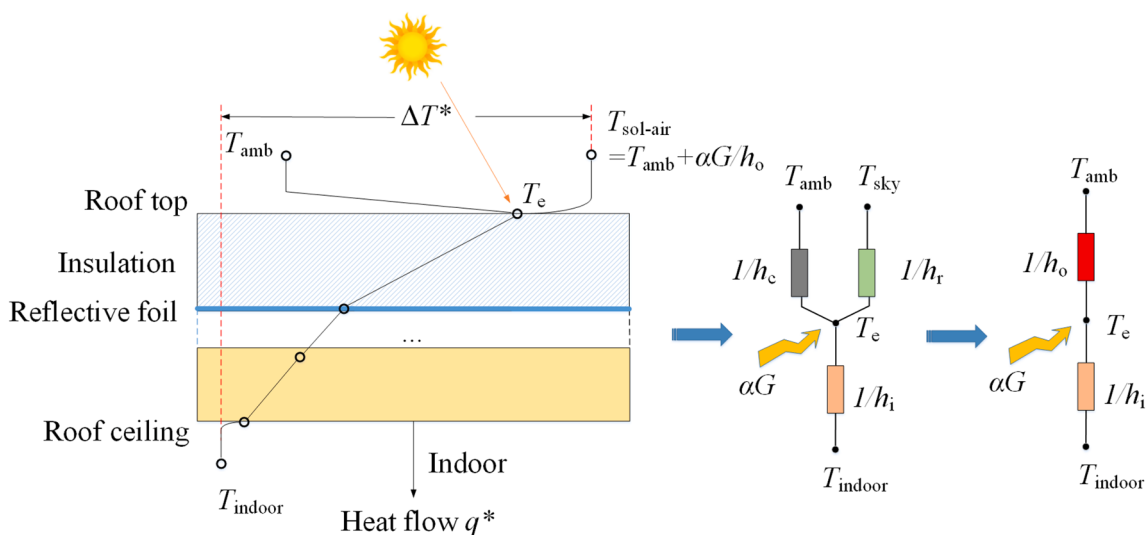


Fig. 16. Roof thermal network for heat flux calculation.

exchange between roof surfaces and indoor or outdoor environment, and the heat conduction through roof multilayers. Cool roof surface with a higher solar reflectivity and thermal emissivity can effectively restrain the process of radiative heat transfer, thus reducing the roof heat gain. The quantitative impacts of roof surface spectral parameters on heat fluxes are significant for the whole building energy performance. To this end, several cool roof-based heat transfer models integrated with roof surface spectral parameters were proposed. Suehrcke et al. (2008) adopted a roof thermal network (Fig. 16) to investigate the impacts of roof solar reflectivity on building heat gains in a hot climate. Equation (12) was utilized to calculate the daily average downward heat gains (HG) through a sunlit roof. When the roof solar absorptance decreased from 0.7 to 0.4, the roof downward heat flux was reduced by 33% and 43% for buildings with or without air conditioners, respectively.

$$HG = \int U \left[(T_{\text{amb}} - T_{\text{indoor}}) + \frac{\alpha G}{h_o} \right] dt \quad (12)$$

where, U is the overall heat transfer coefficient between ambient air and indoor environment, $\text{W}/(\text{m}^2 \cdot \text{K})$; T_{amb} is the ambient temperature, $^{\circ}\text{C}$; T_{indoor} is the indoor temperature, $^{\circ}\text{C}$; α is the solar absorptance; G is the incident solar radiation per unit area, W/m^2 ; h_o is the overall heat transfer coefficient between the roof and ambient air, $\text{W}/(\text{m}^2 \cdot \text{K})$.

A more comprehensive approach has been utilized to analyze the impacts of solar reflectance and thermal emittance on heat fluxes and temperature variations of a multilayered flat roof by using the resistance model in Fig. 17 to analyze the heat transmission process (de Brito Filho et al., 2011). Equations from (13) to (17) consider the time-varying solar radiation and external air temperature. The results indicated that the increase in the roof albedo from 0.3 to 0.9 significantly reduced the roof maximum heat flux from 220 W/m^2 to 50 W/m^2 , and the existence of fiberglass wool could decrease heat fluxes but increase the exterior roof surface temperatures.

$$\frac{T_{\text{amb}}(t) - T_e(t)}{R_e} + \alpha G(t) = \frac{T_e(t) - T_i(t)}{R_{\text{roof}}} \quad (13)$$

$$\frac{T_e(t) - T_i(t)}{R_{\text{roof}}} = \frac{T_i(t) - T_{\text{indoor}}}{R_i} \quad (14)$$

$$R_e = \frac{1}{h_{re} + h_{ce}} \quad (15)$$

$$R_i = \frac{1}{h_{ri} + h_{ci}} \quad (16)$$

$$R_{\text{roof}} = R_1 + R_2 + \dots + R_m = \delta_1/k_1 + \delta_2/k_2 + \dots + \delta_m/k_m \quad (17)$$

where, T_e , T_i are the temperatures of exterior and inner roof surfaces, $^{\circ}\text{C}$; R_e , R_{roof} , R_i are the thermal resistances between external roof surface and outside environment, of roof multilayers and between internal roof surface and indoor environment, $\text{m}^2 \cdot \text{K}/\text{W}$; h_{re} and h_{ce} are the external radiative and convective heat transfer coefficients, $\text{W}/(\text{m}^2 \cdot \text{K})$; h_{ri} and h_{ci} are the internal radiative and convective heat transfer coefficients, $\text{W}/(\text{m}^2 \cdot \text{K})$; δ_m is thickness of "m" roof layer, m ; k_m is heat conductivity coefficient of "m" roof layer, $\text{W}/(\text{m} \cdot \text{K})$.

Zingre and Wan (2013) developed a cool roof heat transfer (CRHT) model for a multilayered roof by using spectral approximation method to obtain the transient heat flux through roof structures. Based on the experimentally validated CRHT model was used to calculate the roof thickness of an uncoated and a thermally insulated roof structures, respectively, which indicated that the cool coating with a high albedo exerted more effects on roof materials with a small R -value ($5\text{--}15 \text{ cm}^2 \cdot \text{K}/\text{W}$). The proposed model was also utilized to predict the thermal performance of a concrete-based cool roof (albedo ~ 0.74), and the results indicated a reduced peak roof temperature of $14.1 \text{ }^{\circ}\text{C}$, indoor air temperature of 2.4

$^{\circ}\text{C}$, and daily heat gain of $0.66 \text{ kWh}/\text{m}^2$ (Zingre et al., 2015a). Additionally, Tong et al. (2014) proposed a Complex Fast Fourier Transform (CFFT) method to calculate the transient roof temperature and heat flux with no need of history temperatures input to save computational efforts.

4.1.2. Roof thermal transfer value (RTTV) model

The RTTV model is an effective method to quantitatively predict roof heat gains or losses for the evaluation of the roof thermal performance. Wong et al. (2003) calculated the peak RTTV for different types of roofs including typical flat roofs with or without vegetation for a five-story commercial building. The RTTV model basically considers three components including the heat conduction through the roof opaque portion, the skylight portion and the solar radiation gains through the roof skylight portion. The results showed rooftop gardens with shrubs provided the most significant reduction in peak RTTV (81%). Based on the aforementioned CRHT model in (Zingre et al., 2015a), Zingre et al. (2015b) further proposed a new RTTV model which considered a new formulation to model the equivalent thermal resistance caused by the

Table 5
Summary of building energy savings benefited from cool roof applications.

Author	Building type	Location	Energy performance
Parker et al. (1998)	Residential house	Florida, USA	Daily electricity savings: 5.4 to $138 \text{ Wh}/\text{m}^2$ (2–45%); Daily peak power reductions: 1.5 to $7.8 \text{ W}/\text{m}^2$ (12–23%)
Akbari et al. (1997)	A house and two school bungalows	Sacramento, California, USA	Cooling energy savings: $2.2 \text{ kWh}/\text{d}$ (house) and $3.1 \text{ kWh}/\text{d}$ (bungalows); Peak demand reduction: 0.6 kW (House and bungalow)
Konopacki et al. (1998)	Two medical offices and a retail store	California, USA	Daily electricity savings: 13–18% (medical offices) and 2% (retail office)
Akbari et al. (2005)	A retail store, a school, and a cold storage building	California, USA	Daily energy savings: $72 \text{ Wh}/\text{m}^2$ (52%)-retail store; $42\text{--}48 \text{ Wh}/\text{m}^2$ (17–18%)-school; $57\text{--}81 \text{ Wh}/\text{m}^2$ (3–4%)-cold storage building
Gao et al. (2014)	Standard compliant office and residential buildings	China	Annual energy savings: 4.1–10.2 kWh/m^2 (numerically); Daily energy savings: 9% (experiments in Chongqing)
Gao et al. (2017)	An office building	Chongqing, China	Daily electricity saving: $0.087 \text{ kWh}/\text{m}^2$ (20.5%); Winter heating penalty: 2.7%; Annual power saving: $3.9 \text{ kWh}/\text{m}^2$
Qiu et al. (2018)	An office building	Shanghai, China	Roof heat gain reduction: 86.9% (a hybrid roof); Reduced thermal insulation layer : 14–107 mm
Kolokotroni et al. (2013)	An office building	London, UK	Annual energy savings: 1–8% (numerically)
Kolokotsa et al. (2012)	A laboratory building	Irkaklion, Greece	Annual energy saving: 19.8%
Synnefa et al. (2012)	A school building	Athens, Greece	Annual cooling energy saving: 40%; Annual heating penalty: 10%
Romeo and Zinzi (2013)	A non-residential building	Sicily, Italy	Cooling load saving: 54%
Touchaei et al. (2016)	Commercial buildings	Montreal, Canada	Annual energy saving: 11% (maximum)
Yang et al. (2018)	An office building	Singapore	Roof heat gain reduction: $15.53 \text{ kWh}/\text{m}^2$ (37%)

solar reflectance of opaque roofs. The proposed RTTV model by incorporating the effects of the surface albedo into U -value overcame the limitations of the former RTTV model's failure to capture solar heat gains with different roof solar reflectances, thus drastically improving the accuracy of RTTV models with the maximum error below 12%. More recently, Fang et al. (2019) proposed an improved RTTV (iRTTV) model by incorporating the roof surface spectral selectivity and thermal mass effects. The model has been validated by a chamber experiment using the daytime cooling film in (Zhai et al., 2017), which exhibited the cooling electricity savings ranging from 113.0 to 143.9 kWh/(m²·yr) relative to shingle roofs.

4.2. Energy and thermal performance

4.2.1. Building energy savings

Numerous studies have documented positive cooling load savings benefited from cool roof implementations both experimentally and numerically. Basically, the savings from cool roofs are related to many factors including geographical climate conditions, roof insulations, duct locations, coating spectral properties, and building types. The early field tests were mainly carried out in America focusing on average and peak cooling energy savings. Due to the apparent energy saving potentials, cool roof studies were rapidly spread into other countries as summarized in Table 5. The combined effects of R -value, cool roof albedo and thermal emittance on heat gains and losses were concurrently considered in (Gentle et al., 2011). Considering the energy savings by increasing R -values under the high albedo were below 2 kWh/(100 m²) per day, the simulation results exhibited that thinner sub-roof insulation layers ($R \leq 1.63$) plus the high albedo and thermal emittance of roof surfaces were more preferable from the thermal and cost perspective. Testa and Krarti (2017) pointed out that the standard commercial roof materials have the solar reflectance varying from 0.05 to 0.36, while typical aged cool roofs have larger albedos ranging from 0.55 to 0.65. Based on cool roof applications in the U.S., the typical energy savings ranged from 0.1 to 8.6 kWh/m², 1.1 to 8.2 kWh/m² and 1.4 to 10.9 kWh/m² for residential, office and retail buildings, respectively. Furthermore, Miller et al. (2002) estimated that the achievable cool roof-based energy saving rates in 240 regions in the U.S. ranged from 12 to 25%, 5 to 18% and 7 to 17% for residential, office and commercial buildings, respectively.

In addition to the abovementioned traditional bulk materials-based cool roof applications, the small-scale experimental tests with daytime radiative cooling materials as roof surfaces were preliminarily conducted to exhibit more cooling potentials. Gentle and Smith (2015) proposed a supercool roof by using the spectrally selective birefringent polymer (solar reflectance ~ 0.97 and selective thermal emittance ~ 0.96). Test results showed the supercool roof could achieve sub-ambient temperature of 2 °C under no convective shield and 11 °C below a commercial cool roof material (solar reflectance ~ 0.74, thermal emittance ~ 0.90). More recently, Fang et al. (2019) proposed a new cool roof using the glass-polymer hybrid metamaterial film in (Zhai et al., 2017) and conducted chamber tests for the validation of a roof thermal transfer model. The study found that the new cool roof could dissipate indoor heat from 137.6 to 268.7 kWh/m² annually into outdoor environment, achieving yearly cooling electricity savings from 113.0 to 143.9 kWh/m² relative to shingle roofs. The simulation-based energy performance using the recently proposed daytime radiative coolers as rooftop super-cool materials was also evaluated. Baniassadi et al. (2019) quantified the potential benefits of applying porous polymer coating in (Mandal et al., 2018b) on building rooftops by conducting the whole-building energy simulation for archetypical residential and commercial buildings located in 8 U.S. cities. The results found that the cooling energy saving as well as heating energy penalties brought by the new super-cool roof could be doubled compared to typical white roofs (solar reflectance ~ 0.7, thermal emittance ~ 0.9). Moreover, a simulation-based comparison method was proposed in (Yu and Chen, 2020) to compare four excellent daytime radiative coolers in (Mandal et al.,

Table 6
Summary of thermal performance benefited from cool roof applications.

Author	Building type	Location	Indicators of thermal performance
Gao et al. (2014)	An office building and a factory	Chongqing and Foshan, China	T_e reductions: 20 °C (Chongqing) and 17 °C (Foshan); T_{indoor} reductions: 1–3 °C (Foshan)
Gao et al. (2017)	Office buildings	Chongqing, China	Average T_{indoor} reductions: 2.5 °C (green roof); 2.7 °C (white roof)
Qiu et al. (2018)	An office building	Shanghai, China	Reductions in T_e : 15 °C; T_i : 1.5 °C; T_{indoor} : 1.0 °C (a hybrid roof)
Synnefa et al. (2007a)	Residential buildings	27 cities, worldwide	Hours of discomfort reductions: 9–100%; Maximum T_{indoor} reductions: 1.2–3.3 °C
Bozonnet et al. (2011)	A duplex flat	Poitiers, France	T_e reduction: over 10 °C
Kolokotroni et al. (2013)	An office building	London	Operative T_{indoor} reduction: 2.5 °C
Dabaieh et al. (2015)	Residential buildings	Cairo, Egypt	Hours of discomfort reduction: 53% (a solar reflective vault roof)
Garg et al. (2016)	Two school buildings	Hyderabad and Nagpur, India	Average T_{indoor} reductions: 2.1 °C (Hyderabad) and 1.5 °C (Nagpur); Peak T_{indoor} reductions: 4.3 °C (Hyderabad) and 3.3 °C (Nagpur)
Kolokotroni et al. (2018)	A single storey house	Jamaica	T_i reduction: 6.8 °C; T_{indoor} reduction: 2.3 °C

2018b; Raman et al., 2014; Zhai et al., 2017; Zhao et al., 2019c) under six standard atmosphere models (Eriksson and Granqvist, 1982). By only considering the emissive power and absorbed radiation, the porous polymer coating in (Mandal et al., 2018b) with the cooling power ranging from 20 to 60 W/m² showed the most cooling potential among four radiative coolers.

4.2.2. Thermal comfort improvement

The benefits of cool roofs can be extended to thermal comfort improvement for naturally ventilated buildings, particularly for those with poorly insulated roof structures (Chen and Lu, 2021). The indicators to evaluate the thermal comfort include the indoor air temperature T_{indoor} , and hours of discomfort. Actually, cool roof applications on the thermal performance improvement have been extensively investigated with some reports summarized in Table 6, which indicates that the average indoor air temperatures can be basically reduced by up to 3 °C from cool roof implementations on naturally ventilated buildings. Such passive cooling method without the need of electricity input to fulfill the thermal comfort is much-anticipated for buildings with poor envelopes in hot climate regions. Hence,

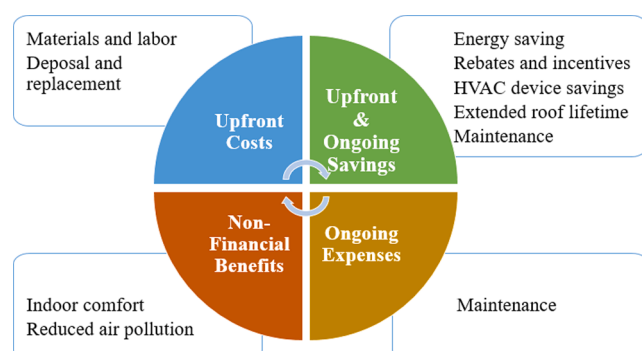


Fig. 18. Components of cool roof life cycle assessment.

Kolokotroni et al. (2018) conducted a field test in a single storey house with or without cool roof paints in Jamaica, which showed that the internal ceiling and air temperatures were decreased by 6.8 and 2.3 °C, respectively. Based on the validated simulations, the study was further extended to low income houses in Recife and Ghana with strong incident solar radiation. The results exhibited that the interior ceiling and indoor air temperatures in the above regions were respectively reduced by 3.2–5.5 °C and 0.75–1.2 °C on average.

4.3. Economic and environmental benefits

4.3.1. Economic assessment

Since cool roof applications induce many positive benefits including the extended roof life span, reduced cooling loads and peak power demands, and the alleviation of urban heat island issues, detailed economic analysis on the overall life cycle assessment (Fig. 18) will provide necessary supports for the promotion of cool roof implementations (Alliances, 2012). To this end, a 50-year life-cycle cost analysis (LCCA) was conducted based on the data collections from 22 flat roof projects in America (Sproul et al., 2014), where the white, green and black roofs were compared to determine the cost effectiveness. The roof net savings (NS) which consider the installation, replacement and maintenance costs, cooling savings, heating penalties, A/C downsizing benefits and avoided power plant emissions were calculated by Equation (18). The results indicated that compared to black roofs, white roofs showed a 50-year net saving of \$25/m² while green roofs which failed to counteract the installation cost premium exhibited a negative net saving of \$71/m². Concerning cooling effects and global warming alleviation, white cool roofs prove more effective than green roofs.

$$NS_{xy} = \sum_{t=0}^N \frac{S_{xy,t}(1+e_s)^t}{(1+d)^t} - \sum_{t=0}^N \frac{C_{xy,t}(1+e_c)^t}{(1+d)^t} \quad (18)$$

where, $S_{xy,t}$ and $C_{xy,t}$ are the saving and cost differences in year t , d is the intergenerational real discount rate, e_s and e_c are the annual fuel price escalation rates for savings and costs, and N is the number of years in the life cycle.

Similarly, Shi et al. (2019) conducted a 40-year life-cycle cost analysis by retrofitting grey roofs with white roofs and sedum-tray garden roofs for office buildings in China. The results found that the white roof has positive net savings of 5.7–35.1 CNY/m² in warm winter climate zones, while by contrast the sedum-tray garden roof showed negative net savings of –81.3 to –16.7 CNY/m² across all climate zones. Thus white roofs were recommended to be applied in office buildings in hot and warm climate zones in China. Additionally, Fang et al. (2019) analyzed the economic savings by using the metamaterial in (Zhai et al., 2017) as cool roofs in cities of Tucson, Los Angeles, Orlando of America. In comparison to the shingle roof, the new cool roof could achieve annual cost savings of \$12.9–\$18.9 /m² and \$10.0–\$18.4 /m² relative to the shingle and thermoplastic polyolefin-based roofs, respectively. With respect to the net economic benefits of using the porous polymer radiative cooler in (Mandal et al., 2018b) as super-cool roofs, Baniassadi et al. (2019) pointed out that the new design has twice the cost saving potential of a conventional white roof.

4.3.2. Urban heat island amelioration

The increase in solar reflectance of urban surfaces will incur an effect of “negative radiative forcing” in which the outflow of reflected solar radiation increases whilst the absorbed heat decreases, resulting in lower surface temperatures to mitigate the local urban heat island (UHI) intensity (Akbari and Matthews, 2012). Meteorological modeling is usually adopted to evaluate impacts of surface albedos on the urban heat island intensity. Actually, both experiments and modeling methods have been utilized to study correlations between surface albedos and ambient temperatures (Pisello, 2017).

For local scale studies, Zingre et al. (2014) established a CFD model

of a building to calculate the air temperatures above the roof so as to investigate impacts of cool roof coatings on microclimate. The maximum air temperature reductions of 1.0, 0.7, 0.6 °C at the height of 0.5, 1.0 and 1.5 m above the roof were achieved under the albedo of 0.8. Moreover, Wray and Akbari (2008) conducted field experiments to measure the rooftop outdoor air near the condenser inlet which was found to be reduced by 0.3 °C after applying the cool roof. Yang et al. (2018) compared green and cool roof applications in tropical climate, where the heat flux through roof structures was calculated by EnergyPlus to evaluate the positive effects of both strategies for UHI mitigation. Regarding city-scale investigations, Savio et al. (2006) detected the urban air temperatures in New York city with considering the solar reflectance of 0.5 and found that temperature reductions ranged from 0.18 to 0.36 K on average. Synnefa et al. (2008) performed numerical simulations by using nonhydrostatic MM5 to assess the impacts of albedo increases on ambient temperatures in building rooftops in the city of Athens, Greece. Two albedos were studied with the results showing that the temperature depressions were 1.5 °C (albedo 0.63) and 2.2 °C (albedo 0.85) at the height of 2 m, indicating the heat island intensity could be reduced by 1–2 °C by using high surface albedo strategies. Millstein and Menon (2011) conducted the investigation on regional climate by changing surface albedos to mimic cool roofs across the United States. The results showed that noontime temperatures in urban areas were reduced by 0.11–0.53 °C, while by contrast rural areas showed a temperature increase over 0.27 °C due to less precipitation and cloud cover. The above studies shed light on the positive potential of cool roofs to reduce the urban heat island intensity.

4.3.3. Carbon emission reduction

Since cool roofs can bring noticeable energy savings in buildings, the energy consumption from fossil fuels which are responsible for a large portion of carbon emissions can be reduced accordingly. Xu et al. (2012) quantified cooling load savings of cool roof applications for commercial buildings by developing a field-based analytical method. The results showed that direct CO₂ reductions of 11–12 kg/m² of flat roof areas could be achieved. More broadly, Akbari et al. (2009) pointed out that roofs (20–25%) and pavements (40%) account for the urban surfaces >60%, the albedos of which can be improved by 0.25 and 0.15 respectively which may offset equivalent CO₂ emissions of 44 Gt globally. The further study showed carbon equivalent offset about 40–160 Gt could be achieved which equal to about \$1–4 trillion according to the CO₂ price of \$25/t (Akbari and Matthews, 2012). Millstein and Menon (2011) also reported the reduced carbon emission from cool roof strategies. They investigated the regional climate variations by the Weather Research and Forecasting (WRF) model. The results exhibited that cool roofs and pavements increase the annual outgoing thermal radiation by 0.16 ± 0.03 W/m² offsetting 3.3 ± 0.5 Gt CO₂. More recently, Baniassadi et al. (2019) calculated the net CO₂ emissions by applying porous polymer coating reported in (Mandal et al., 2018b) on residential and commercial building rooftops in 8 U.S. cities and gave that this super-cool roof design could double the benefits of conventional white roofs for the avoidance of CO₂ emissions. As an alternative geoengineering approach, radiative cooling technology can be part of a complete portfolio of measures to counter the global warming by reducing the energy consumption in buildings to decrease CO₂ emissions and simultaneously inducing a negative radiative forcing to cool the earth's surface (Akbari et al., 2009; Munday, 2019), while further detailed techno-economic analysis in this respect is needed.

To sum up, radiative roof cooling has been widely investigated regarding its profound impacts on building energy and thermal performance, as well as subsequent benefits on economy, and city-wide microclimate. The cool roof-based heat transfer models accounting for additional heat insulation capacity have also been studied. Nevertheless, in practical cool roof implementations, the concomitant issues regarding heating penalties in cold regions, the visual discomfort caused by bright glaring white roofs and reflectance degradations (Council and Directory,

2019) due to dust or pollutant accumulations should be discreetly taken into account. Actually, heating penalties can be readily addressed by distinguishing the favored climate regions, like climates with a long cooling but a short heating season, or using coatings with switchable spectral properties during different seasons (Testa and Krarti, 2017). Since direct silvered designs (Gentle and Smith, 2015; Raman et al., 2014; Zhai et al., 2017) as roof surfaces to achieve high solar reflectances unavoidably cause strong glare due to specular or semi-specular reflections, which may harm eyesight and be undesirable for neighboring higher buildings, a possible way to address the issue whilst still preserve the cooling capacity would be to introduce a retroreflective surface to return sunlight to its source (Levinson et al., 2020; Qin et al., 2016; Rossi et al., 2016; Rossi et al., 2015; Yuan et al., 2016), like coating super-white radiative coolers with commercial high index ($n \sim 1.9$) retroreflective spheres (Mandal et al., 2020) to reflect sunlight into sky, which remains for further exploration. It should be noted that due to building rooftops typically maintain at near or above ambient temperatures because of direct contact with air and heat generation indoors, a broadband thermal emitter can be similarly effective at cooling as a spectrally selective emitter. Moreover, now that most non-metallic materials intrinsically exhibit a high and broadband emissivity, broadband emitters are currently more suitable and outweighing spectrally selective emitters for practical applications on building rooftops (Mandal et al., 2020). It is also worth noting that due to the burgeoning daytime radiative cooling materials or designs being reported with the excellent solar reflectance and thermal emittance (e.g. $\beta \sim 0.98$ and $\epsilon \sim 0.97$ in (Mandal et al., 2018b)), which are much higher than traditionally commercial cool paints (e.g. β less than 0.86 for the best TiO₂-based paints (Mandal et al., 2020)), the implementations of the new materials as cool roofs can potentially bring more practical benefits both economically and environmentally. Hence, more thermal and energy performance evaluations based on the newly emerging cooling designs as building rooftops are necessary for further investigation.

5. Conclusions and prospects

In this paper, a critical review concerning the radiative cooling and its potential integration with buildings is comprehensively provided. First of all, the fundamentals of radiative cooling were analyzed in detail, where the extensive parametric analyses were conducted regarding the impacts of different types of radiative coolers, the atmospheric water vapors and the non-radiative heat transfer components on the achievable equilibrium temperature and the net cooling power. Afterwards, various radiative cooling material designs were detailed comprehensively. The practical achievement of daytime radiative cooling is largely attributed to the realization of material designs with the excellent solar reflectance together with tailored infrared spectral selectivity within the atmospheric transparency window. The applications of radiative cooling are tremendously diverse, including building-integrated radiative cooling for energy savings, solar cell cooling for efficiency improvement, and other promising exploitations. Radiative cooling has great potential to be integrated with buildings in variety of ways either by direct or indirect forms for the ultimate goals of indoor thermal comfort and energy savings. Cool roof is a typical example of direct implementations of radiative cooling in buildings. Cool roof strategies as the most direct and mature way to implement the radiative cooling in buildings are conducive to fulfilling energy savings and indoor thermal comfort and melioration of urban microclimate. It is worth noting that passive radiative cooling belongs to a low-energy technology, and thus if it is integrated with buildings either by combining with power supply systems or in the form of cool roofs, large roof areas are entailed to fulfil substantial building cooling demands. To facilitate the large-scale systematic applications of radiative cooling, the key research directions are envisaged as follows:

- 1) More advanced radiative cooling material designs with less complex structures, low-cost and large-scale manufacturability. Specifically, the scalable adaptive radiative cooling designs with tuneable spectral properties of solar reflectance and thermal emittance in accordance with seasonal temperature variations are yet to be further explored with excellent daytime cooling capability.
- 2) Durability and resistance to soiling. Soiling poses a challenge for all passive daytime radiative coolers (Mandal et al., 2020) due to the gradually reduced solar reflectance over time when exposure to external environment. The impacts of dust and other particulate matters settling on radiative coolers on the degradation of spectral properties and cooling performance are essentially entailed for further investigation. More advanced designs that are resistant to soiling, such as hydrophobic topcoats, should be deeply explored to lengthen and strengthen cooling capacity.
- 3) Experimental study on the integration of daytime radiative cooling with building power supply systems. Current combinations of these hybrid systems to achieve energy savings are conceptually proposed or numerically studied, which need to be further experimentally investigated and validated.
- 4) A robust energy storage system to ensure a stable and efficient energy conversion. The intrinsic low-energy density and stochastic characteristics of radiative cooling require good energy storage systems for smooth operations, especially for those working during the daytime while performing power storage during the nighttime periods.
- 5) Performance evaluation of radiative roof cooling by integrating spectral properties of newly emerging excellent daytime cooling materials with the strong solar reflectance and thermal emittance. Studies on cool roof benefits regarding the thermal and energy performance, urban heat island mitigation have long been constrained to traditional bulk materials without adequate daytime cooling capability. Hence, more remarkable benefits will be achieved across different climate regions by adopting daytime radiative cooling designs, like new paints in (Mandal et al., 2020).
- 6) Correlations establishment between meteorological parameters and the cooling capacity of radiative cooling materials. Since radiative cooling potential is substantively dependent on local climatic conditions, the established correlations across the world will facilitate radiative cooling implementations globally, such as the work done across the United States to characterize thermal radiant temperatures (Martin and Berdahl, 1984), energy uses (Levinson and Akbari, 2010) and radiative cooling resource maps (Li et al., 2019a).
- 7) Policy studies with attractive rebate schemes or financial incentives regarding radiative cooling implementations in local buildings as an impetus to facilitate such renewable energy utilization technology.

Declaration of Competing Interest

The authors declared that there is no conflict of interest.

Acknowledgement

The work is partially supported by Hong Kong Research Grant Council through General Research Fund (PolyU 152184/17E).

References

- Abdollahramezani, S., Hemmatyar, O., Taghinejad, H., et al., 2020. Tunable nanophotonics enabled by chalcogenide phase-change materials. *Nanophotonics* 9 (5), 1189–1241.
- Aili, A., Wei, Z.Y., Chen, Y.Z., et al., 2019. Selection of polymers with functional groups for daytime radiative cooling. *Materials Today: Physics* 10.
- Akbari, H., Bretz, S., Kurn, D.M., et al., 1997. Peak power and cooling energy savings of high-albedo roofs. *Energy Build.* 25 (2), 117–126.
- Akbari, H., Levinson, R., 2008. Evolution of cool-roof standards in the US. *Adv. Build. Energy Res.* 2 (1), 1–32.
- Akbari, H., Levinson, R., Rainer, L., 2005. Monitoring the energy-use effects of cool roofs on California commercial buildings. *Energy Build.* 37 (10), 1007–1016.

- Akbari, H., Matthews, H.D., 2012. Global cooling updates: Reflective roofs and pavements. *Energy Build.* 55, 2–6.
- Akbari, H., Menon, S., Rosenfeld, A., 2009. Global cooling: increasing world-wide urban albedos to offset CO₂. *Clim. Change* 94 (3), 275–286.
- Ali, A.H.H., 2007. Passive cooling of water at night in uninsulated open tank in hot arid areas. *Energy Convers. Manage.* 48 (1), 93–100.
- Alliances, G.C.C., 2012. A Practical Guide to cool roofs and cool pavements.
- Andretta, A., Bartoli, B., Coluzzi, B., et al., 1981. Selective Surfaces For Natural Cooling Devices. *J. Phys. Colloques*, 42(C1): C1-423-C1-430.
- Ao, X., Hu, M., Zhao, B., et al., 2019. Preliminary experimental study of a specular and a diffuse surface for daytime radiative cooling. *Sol. Energy Mater. Sol. Cells* 191, 290–296.
- Atiganyanun, S., Plumley, J.B., Han, S.J., et al., 2018. Effective radiative cooling by paint-format microsphere-based photonic random media. *ACS Photonics* 5 (4), 1181–1187.
- Bainbridge, D., Haggard, K., 2011. Passive solar architecture: heating, cooling, ventilation, daylighting and more using natural flows. Chelsea green publishing.
- Baniassadi, A., Sailor, D.J., Ban-Weiss, G.A., 2019. Potential energy and climate benefits of super-cool materials as a rooftop strategy. *Urban Clim.* 29.
- Bao, H., Yan, C., Wang, B., et al., 2017. Double-layer nanoparticle-based coatings for efficient terrestrial radiative cooling. *Sol. Energy Mater. Sol. Cells* 168, 78–84.
- Bartoli, B., Catalano, S., Coluzzi, B., et al., 1977. Nocturnal and diurnal performances of selective radiators. *Appl. Energy* 3 (4), 267–286.
- Bathgate, S.N., Bosi, S.G., 2011. A robust convection cover material for selective radiative cooling applications. *Sol. Energy Mater. Sol. Cells* 95 (10), 2778–2785.
- Bedford, R.G., Triplett, G., Tomich, D.H., et al., 2011. Reduced auger recombination in mid-infrared semiconductor lasers. *J. Appl. Phys.* 110 (7), 073108.
- Benlattar, M., Oualim, E.M., Harmouchi, M., et al., 2005. Radiative properties of cadmium telluride thin film as radiative cooling materials. *Opt. Commun.* 256 (1), 10–15.
- Berdahl, P., 1984. Radiative cooling with MgO and/or LiF layers. *Appl. Opt.* 23 (3), 370–372.
- Berdahl, P., Boocock, S.K., Chan, G.C.Y., et al., 2018. High quantum yield of the Egyptian blue family of infrared phosphors (MCuSi₄O₁₀, M = Ca, Sr, Ba). *J. Appl. Phys.* 123 (19).
- Berdahl, P., Bretz, S.E., 1997. Preliminary survey of the solar reflectance of cool roofing materials. *Energy Build.* 25 (2), 149–158.
- Berdahl, P., Chen, S.S., Destailhats, H., et al., 2016. Fluorescent cooling of objects exposed to sunlight – The ruby example. *Sol. Energy Mater. Sol. Cells* 157, 312–317.
- Berk, A., Anderson, G.P., Acharya, P.K., et al., 2006. MODTRAN5: 2006 update. SPIE Defense and Security Symposium.
- Boudet, T., Chaton, P., Herault, L., et al., 1996. Thin-film designs by simulated annealing. *Appl. Opt.* 35 (31), 6219–6226.
- Bozonnet, E., Doya, M., Allard, F., 2011. Cool roofs impact on building thermal response: A French case study. *Energy Build.* 43 (11), 3006–3012.
- Brady, R.F., Wake, L.V., 1992. Principles and formulations for organic coatings with tailored infrared properties. *Prog. Org. Coat.* 20 (1), 1–25.
- Byrnes, S.J., Blanchard, R., Capasso, F., 2014. Harvesting renewable energy from Earth's mid-infrared emissions. *Proc. Natl. Acad. Sci. USA* 111 (11), 3927–3932.
- Catalano, S., Cuomo, V., Piro, G., et al., 1975. The radiative cooling of selective surfaces. *Sol. Energy* 17 (2), 83–89.
- Chandrasekhar, P., Zay, B.J., Lawrence, D., et al., 2014. Variable-emittance infrared electrochromic skins combining unique conducting polymers, ionic liquid electrolytes, microporous polymer membranes, and semiconductor/polymer coatings, for spacecraft thermal control. *J. Appl. Polym. Sci.* 131 (19), n/a-n/a.
- Chen, J., Lu, L., 2021. Comprehensive evaluation of thermal and energy performance of radiative roof cooling in buildings. *J. Build. Eng.* 33, 101631.
- Chen, Y., Mandal, J., Li, W., et al., 2020. Colored and paintable bilayer coatings with high solar-infrared reflectance for efficient cooling. *Sci. Advances* 6 (17), eaaz5413.
- Chen, Z., Zhu, L., Raman, A., et al., 2016. Radiative cooling to deep sub-freezing temperatures through a 24-h day-night cycle. *Nat. Communications* 7, 13729.
- Cheng, C.-L., 2002. Study of the inter-relationship between water use and energy conservation for a building. *Energy Build.* 34 (3), 261–266.
- Cheung, C.T., Mui, K.W., Wong, L.T., 2013. Energy efficiency of elevated water supply tanks for high-rise buildings. *Appl. Energy* 103, 685–691.
- Chung, M.H., Park, J.C., 2016. Development of PCM cool roof system to control urban heat island considering temperate climatic conditions. *Energy Build.* 116, 341–348.
- Cool Roof Rating Council. Rated Products Directory. [cited 2019 12 December]; Available from: <https://coolroofs.org/directory>.
- Cui, Y., He, Y., Jin, Y., et al., 2014. Plasmonic and metamaterial structures as electromagnetic absorbers. *Laser Photonics Rev.* 8 (4), 495–520.
- Cui, Y., Xu, J., Fung, K.H., et al., 2011. A thin film broadband absorber based on multi-sized nanoantennas. *Appl. Phys. Lett.* 99 (25), 253101.
- Czapla, B., Srinivasan, A., Yin, Q., et al., 2017. Potential for Passive Radiative Cooling by PDMS Selective Emitters, ASME 2017 Heat Transfer Summer Conference.
- Dabaieh, M., Wanis, O., Hegazy, M.A., et al., 2015. Reducing cooling demands in a hot dry climate: A simulation study for non-insulated passive cool roof thermal performance in residential buildings. *Energy Build.* 89, 142–152.
- de Brito Filho, J., Henriquez, J., Dutra, J., 2011. Effects of coefficients of solar reflectivity and infrared emissivity on the temperature and heat flux of horizontal flat roofs of artificially conditioned nonresidential buildings. *Energy Build.* 43 (2–3), 440–445.
- Diatezua, D.M., Thiry, P.A., Dereux, A., et al., 1996. Silicon oxynitride multilayers as spectrally selective material for passive radiative cooling applications. *Sol. Energy Mater. Sol. Cells* 40 (3), 253–259.
- Dimoudi, A., Androutopoulos, A., 2006. The cooling performance of a radiator based roof component. *Sol. Energy* 80 (8), 1039–1047.
- Dobson, K.D., Hodes, G., Mastai, Y., 2003. Thin semiconductor films for radiative cooling applications. *Sol. Energy Mater. Sol. Cells* 80 (3), 283–296.
- Eicker, U., Dalibard, A., 2011. Photovoltaic-thermal collectors for night radiative cooling of buildings. *Sol. Energy* 85 (7), 1322–1335.
- El-Kady, I., Farfan, G.B., Rammohan, R., et al., 2008. Photonic crystal high-efficiency multispectral thermal emitters. *Appl. Phys. Lett.* 93 (15), 153501.
- ENERGY STAR. Certified Roof Products [cited 2019 12 December]; Available from: https://www.energystar.gov/products/building_products/roof_products.
- Erell, E., Etzion, Y., 1999. Analysis and experimental verification of an improved cooling radiator. *Renewable Energy* 16 (1), 700–703.
- Eriksson, T.S., Granqvist, C.G., 1982. Radiative cooling computed for model atmospheres. *Appl. Opt.* 21 (23), 4381–4388.
- Eriksson, T.S., Jiang, S.J., Granqvist, C.G., 1985. Surface coatings for radiative cooling applications: silicon dioxide and silicon nitride made by reactive rf-sputtering. *Solar Energy Materials* 12 (5), 319–325.
- Eriksson, T.S., Lushiku, E.M., Granqvist, C.G., 1984. Materials for radiative cooling to low temperature. *Solar Energy Materials* 11 (3), 149–161.
- Fang, H., Zhao, D., Yuan, J., et al., 2019. Performance evaluation of a metamaterial-based new cool roof using improved Roof Thermal Transfer Value model. *Appl. Energy* 248, 589–599.
- Farmahini-Farahani, M., Heidarnejad, G., 2012. Increasing effectiveness of evaporative cooling by pre-cooling using nocturnally stored water. *Appl. Therm. Eng.* 38, 117–123.
- Farmahini Farahani, M., Heidarnejad, G., Delfani, S., 2010. A two-stage system of nocturnal radiative and indirect evaporative cooling for conditions in Tehran. *Energy Build.* 42 (11), 2131–2138.
- Fernández, J.J., 2020. Emissive-energy harvesting using near-field heat transfer. *Engineering Research Express* 2 (1), 015040.
- Fixsen, D., 2009. The temperature of the cosmic microwave background. *Astrophys J* 707 (2), 916.
- Fleming, J.G., Lin, S.Y., El-Kady, I., et al., 2002. All-metallic three-dimensional photonic crystals with a large infrared bandgap. *Nature* 417 (6884), 52–55.
- Fu, Y., Yang, J., Su, Y.S., et al., 2019. Daytime passive radiative cooler using porous alumina. *Sol. Energy Mater. Sol. Cells* 191, 50–54.
- Gao, Y., Shi, D., Levinson, R., et al., 2017. Thermal performance and energy savings of white and sedum-tray garden roof: A case study in a Chongqing office building. *Energy Build.* 156, 343–359.
- Gao, Y., Xu, J., Yang, S., et al., 2014. Cool roofs in China: Policy review, building simulations, and proof-of-concept experiments. *Energy Policy* 74, 190–214.
- Garg, V., Kotharkar, R., Sathaye, J., et al., 2016. Assessment of the impact of cool roofs in rural buildings in India. *Energy Build.* 114, 156–163.
- Gemini Observatory. IR transmission spectra. [cited 2019 September 15]; Available from: <http://www.gemini.edu/sciops/telescopes-and-sites/observing-condition-constraints/ir-transmission-spectra>.
- Gentle, A., Dybdal, K., Smith, G., 2013. Polymeric mesh for durable infra-red transparent convection shields: applications in cool roofs and sky cooling. *Sol. Energy Mater. Sol. Cells* 115, 79–85.
- Gentle, A.R., Aguilar, J.L.C., Smith, G.B., 2011. Optimized cool roofs: Integrating albedo and thermal emittance with R-value. *Sol. Energy Mater. Sol. Cells* 95 (12), 3207–3215.
- Gentle, A.R., Smith, G.B., 2010. Radiative Heat Pumping from the Earth Using Surface Phonon Resonant Nanoparticles. *Nano Lett.* 10 (2), 373–379.
- Gentle, A.R., Smith, G.B., 2015. A Subambient Open Roof Surface under the Mid-Summer Sun. *Adv. Sci.* 2 (9), 1500119.
- Gentle, A.R., Smith, G.B., 2016. Is enhanced radiative cooling of solar cell modules worth pursuing? *Sol. Energy Mater. Sol. Cells* 150, 39–42.
- Goldstein, E.A., Raman, A.P., Fan, S., 2017. Sub-ambient non-evaporative fluid cooling with the sky. *Nat. Energy* 2 (9).
- Granqvist, C.G., 1981. Radiative heating and cooling with spectrally selective surfaces. *Appl. Opt.* 20 (15), 2606–2615.
- Granqvist, C.G., Hjortsberg, A., 1980. Surfaces for radiative cooling: Silicon monoxide films on aluminum. *Appl. Phys. Lett.* 36 (2), 139–141.
- Granqvist, C.G., Hjortsberg, A., 1981. Radiative cooling to low temperatures: General considerations and application to selectively emitting SiO films. *J. Appl. Phys.* 52 (6), 4205–4220.
- Granqvist, C.G., Hjortsberg, A., Eriksson, T.S., 1982. Radiative cooling to low temperatures with selectivity IR-emitting surfaces. *Thin Solid Films* 90 (2), 187–190.
- Grenier, P., 1979. Réfrigération radiative. Effet de serre inverse. *Rev. Phys. Appl. (Paris)* 14 (1), 87–90.
- Hamza, H., Ali, A., Taha, I.M.S., Ismail, I.M., 1995. Cooling of water flowing through a night sky radiator. *Sol. Energy* 55 (4), 235–253.
- Han, D., Ng, B.F., Wan, M.P., 2020. Preliminary study of passive radiative cooling under Singapore's tropical climate. *Sol. Energy Mater. Sol. Cells* 206, 110270.
- Hanif, M., Mahlia, T.M.I., Zare, A., et al., 2014. Potential energy savings by radiative cooling system for a building in tropical climate. *Renew. Sustain. Energy Rev.* 32, 642–650.
- Harrison, A.W., 1981. Effect of atmospheric humidity on radiation cooling. *Sol. Energy* 26 (3), 243–247.
- Harrison, A.W., Walton, M.R., 1978. Radiative cooling of TiO₂ white paint. *Sol. Energy* 20 (2), 185–188.
- Heat Island Group. The Cool Colors Project. [cited 2020 20 March]; Available from: <https://coolcolors.lbl.gov/>.
- Heidarnejad, G., Farmahini Farahani, M., Delfani, S., 2010. Investigation of a hybrid system of nocturnal radiative cooling and direct evaporative cooling. *Build. Environ.* 45 (6), 1521–1528.

- Hernández-Pérez, I., Álvarez, G., Xamán, J., et al., 2014. Thermal performance of reflective materials applied to exterior building components—A review. *Energy Build.* 80, 81–105.
- Hjortsberg, A., Granqvist, C.G., 1980. Infrared optical properties of silicon monoxide films. *Appl. Opt.* 19 (10), 1694–1696.
- Hjortsberg, A., Granqvist, C.G., 1981. Radiative cooling with selectively emitting ethylene gas. *Appl. Phys. Lett.* 39 (6), 507–509.
- Hossain, M.M., Chen, G., Jia, B., et al., 2010. Optimization of enhanced absorption in 3D-woodpile metallic photonic crystals. *Opt. Express* 18 (9), 9048–9054.
- Hossain, M.M., Gu, M., 2016. Radiative Cooling: Principles, Progress, and Potentials. *Adv. Sci. (Weinh)* 3 (7), 1500360.
- Hossain, M.M., Jia, B., Gu, M., 2015. A Metamaterial Emitter for Highly Efficient Radiative Cooling. *Adv. Opt. Mater.* 3 (8), 1047–1051.
- Hu, M., Pei, G., Wang, Q., et al., 2016. Field test and preliminary analysis of a combined diurnal solar heating and nocturnal radiative cooling system. *Appl. Energy* 179, 899–908.
- Hu, M., Zhao, B., Ao, X., et al., 2018. Field investigation of a hybrid photovoltaic-photothermic-radiative cooling system. *Appl. Energy* 231, 288–300.
- Hu, M., Zhao, B., Li, J., et al., 2017. Preliminary thermal analysis of a combined photovoltaic-photothermic-nocturnal radiative cooling system. *Energy* 137, 419–430.
- Huang, Z., Ruan, X., 2017. Nanoparticle embedded double-layer coating for daytime radiative cooling. *Int. J. Heat Mass Transf.* 104, 890–896.
- Ishad, K., Habib, K., Thirumalaiswamy, N., et al., 2015. Performance analysis of a thermoelectric air duct system for energy-efficient buildings. *Energy* 91, 1009–1017.
- Ishii, S., Dao, T.D., Nagao, T., 2020. Radiative cooling for continuous thermoelectric power generation in day and night. *Appl. Phys. Lett.* 117 (1).
- Jeong, S.Y., Tso, C.Y., Wong, Y.M., et al., 2020. Daytime passive radiative cooling by ultra emissive bio-inspired polymeric surface. *Solar Energy Materials and Solar Cells*, 206.
- Kecibas, M.A., Menguc, M.P., Kosar, A., et al., 2017. Passive radiative cooling design with broadband optical thin-film filters. *J. Quant. Spectrosc. Radiat. Transfer* 198, 179–186.
- Kharrufa, S.N., Adil, Y., 2008. Roof pond cooling of buildings in hot arid climates. *Build. Environ.* 43 (1), 82–89.
- Khedari, J., Waesak, J., Thepa, S., et al., 2000. Field investigation of night radiation cooling under tropical climate. *Renewable Energy* 20 (2), 183–193.
- Kim, H., Cheung, K., Auyeung, R.C.Y., et al., 2019. VO₂-based switchable radiator for spacecraft thermal control. *Sci. Rep.* 9 (1), 11329.
- Kimball, B.A., 1985. Cooling performance and efficiency of night sky radiators. *Sol. Energy* 34 (1), 19–33.
- Knight, M.W., Sobhani, H., Nordlander, P., et al., 2011. Photodetection with Active Optical Antennas. *Science* 332 (6030), 702–704.
- Kolokotroni, M., Gowreesunker, B.L., Giridharan, R., 2013. Cool roof technology in London: An experimental and modelling study. *Energy Build.* 67, 658–667.
- Kolokotroni, M., Shittu, E., Santos, T., et al., 2018. Cool roofs: High tech low cost solution for energy efficiency and thermal comfort in low rise low income houses in high solar radiation countries. *Energy Build.* 176, 58–70.
- Kolokotsa, D., Diakaki, C., Papantoniou, S., et al., 2012. Numerical and experimental analysis of cool roofs application on a laboratory building in Iraklion, Crete, Greece. *Energy Build.* 55, 85–93.
- Konopacki, S., Akbari, H., Gartland, L., 1997. Cooling energy savings potential of light-colored roofs for residential and commercial buildings in 11 US metropolitan areas. Lawrence Berkeley Lab, CA (United States).
- Konopacki, S., Gartland, L., Akbari, H., et al., 1998. Demonstration of energy savings of cool roofs. United States.
- Kou, J.-L., Jurado, Z., Chen, Z., et al., 2017. Daytime Radiative Cooling Using Near-Black Infrared Emitters. *ACS Photonics* 4 (3), 626–630.
- Landro, B., McCormick, P.G., 1980. Effect of surface characteristics and atmospheric conditions on radiative heat loss to a clear sky. *Int. J. Heat Mass Transf.* 23 (5), 613–620.
- Lawrence Berkeley National Laboratory. SRI Calculator. [cited 2020 19 March]; Available from: <https://www.usgbc.org/resources/lawrence-berkeley-national-laboratory-sri-calculator>.
- Lei, J., Kumarasamy, K., Zingre, K.T., et al., 2017. Cool colored coating and phase change materials as complementary cooling strategies for building cooling load reduction in tropics. *Appl. Energy* 190, 57–63.
- Leroy, A., Bhatia, B., Kelsall, C.C., et al., 2019. High-performance subambient radiative cooling enabled by optically selective and thermally insulating polyethylene aerogel. *Science Advances* 5 (10), eaat9480.
- Levinson, R., Akbari, H., 2010. Potential benefits of cool roofs on commercial buildings: conserving energy, saving money, and reducing emission of greenhouse gases and air pollutants. *Energ. Effi.* 3 (1), 53–109.
- Levinson, R., Akbari, H., Berdahl, P., et al., 2010. A novel technique for the production of cool colored concrete tile and asphalt shingle roofing products. *Sol. Energy Mater. Sol. Cells* 94 (6), 946–954.
- Levinson, R., Berdahl, P., Akbari, H., et al., 2007. Methods of creating solar-reflective nonwhite surfaces and their application to residential roofing materials. *Sol. Energy Mater. Sol. Cells* 91 (4), 304–314.
- Levinson, R., Chen, S., Slack, J., et al., 2020. Design, characterization, and fabrication of solar-retroreflective cool-wall materials. *Solar Energy Materials and Solar Cells*, 206.
- Li, L., Wang, Q.H., Li, D.H., et al., 2009. Jump method for optical thin film design. *Opt. Express* 17 (19), 16920–16926.
- Li, M., Peterson, H.B., Coimbra, C.F.M., 2019a. Radiative cooling resource maps for the contiguous United States. *J. Renewable Sustainable Energy* 11 (3).
- Li, T., Zhai, Y., He, S., et al., 2019b. A radiative cooling structural material. *Science* 364 (6442), 760–763.
- Li, W., Fan, S., 2018. Nanophotonic control of thermal radiation for energy applications [Invited]. *Opt. Express* 26 (12), 15995–16021.
- Li, W., Shi, Y., Chen, K., et al., 2017. A Comprehensive Photonic Approach for Solar Cell Cooling. *ACS Photonics* 4 (4), 774–782.
- Li, W., Shi, Y., Chen, Z., et al., 2018. Photonic thermal management of coloured objects. *Nat. Commun.* 9 (1), 4240.
- Liu, C., Wu, Y., Wang, B., et al., 2019a. Effect of atmospheric water vapor on radiative cooling performance of different surfaces. *Sol. Energy* 183, 218–225.
- Liu, J., Zhang, Y., Zhang, D., et al., 2020. Model development and performance evaluation of thermoelectric generator with radiative cooling heat sink. *Energy Convers. Manage.* 216.
- Liu, J., Zhou, Z., Zhang, J., et al., 2019b. Advances and challenges in commercializing radiative cooling. *Materials Today. Physics* 11.
- Liu, X., Starr, T., Starr, A.F., et al., 2010. Infrared Spatial and Frequency Selective Metamaterial with Near-Unity Absorbance. *Phys. Rev. Lett.* 104 (20), 207403.
- Lu, X., Xu, P., Wang, H., et al., 2016. Cooling potential and applications prospects of passive radiative cooling in buildings: The current state-of-the-art. *Renew. Sustain. Energy Rev.* 65, 1079–1097.
- Lu, Y., Chen, Z., Ai, L., et al., 2017. A Universal Route to Realize Radiative Cooling and Light Management in Photovoltaic Modules. *Solar RRL* 1 (10).
- Lushikui, E.M., Granqvist, C.-G., 1984. Radiative cooling with selectively infrared-emitting gases. *Appl. Opt.* 23 (11), 1835–1843.
- Lushikui, E.M., Hjortsberg, A., Granqvist, C.G., 1982. Radiative cooling with selectively infrared-emitting ammonia gas. *J. Appl. Phys.* 53 (8), 5526–5530.
- Ma, W., Wen, Y., Yu, X., 2013. Broadband metamaterial absorber at mid-infrared using multiplexed cross resonators. *Opt. Express* 21 (25), 30724–30730.
- Man, Y., Yang, H., Spitzer, J.D., et al., 2011. Feasibility study on novel hybrid ground coupled heat pump system with nocturnal cooling radiator for cooling load dominated buildings. *Appl. Energy* 88 (11), 4160–4171.
- Mandal, J., Du, S., Dontigny, M., et al., 2018a. Li4Ti5O12: A Visible-to-Infrared Broadband Electrochromic Material for Optical and Thermal Management. *Adv. Funct. Mater.* 28 (36).
- Mandal, J., Fu, Y., Overvig, A.C., et al., 2018b. Hierarchically porous polymer coatings for highly efficient passive daytime radiative cooling. *Science* 362 (6412), 315–319.
- Mandal, J., Jia, M., Overvig, A., et al., 2019. Porous Polymers with Switchable Optical Transmittance for Optical and Thermal Regulation. *Joule* 3 (12), 3088–3099.
- Mandal, J., Yang, Y., Yu, N., et al., 2020. Paints as a Scalable and Effective Radiative Cooling Technology for Buildings. *Joule* 4 (7), 1350–1356.
- Martin, M., Berdahl, P., 1984. Characteristics of infrared sky radiation in the United States. *Sol. Energy* 33 (3–4), 321–336.
- Matsuta, M., Terada, S., Ito, H., 1987. Solar heating and radiative cooling using a solar collector-sky radiator with a spectrally selective surface. *Sol. Energy* 39 (3), 183–186.
- Meir, M.G., Rekstad, J.B., Løvvik, O.M., 2002. A study of a polymer-based radiative cooling system. *Sol. Energy* 73 (6), 403–417.
- Michell, D., Biggs, K.L., 1979. Radiation cooling of buildings at night. *Appl. Energy* 5 (4), 263–275.
- Mihalakakou, G., Ferrante, A., Lewis, J.O., 1998. The cooling potential of a metallic nocturnal radiator. *Energy Build.* 28 (3), 251–256.
- Miller, W., Cheng, M., Pfiffner, S., et al., 2002. The Field Performance of High-Reflectance Single-Ply Membranes Exposed to Three Years of Weathering in Various US Climates. Final Report to SPRI, Inc., August.
- Millstein, D., Menon, S., 2011. Regional climate consequences of large-scale cool roof and photovoltaic array deployment. *Environ. Res. Lett.* 6 (3), 034001.
- Mu, E., Wu, Z., Wu, Z., et al., 2019. A novel self-powering ultrathin TEG device based on micro/nano emitter for radiative cooling. *Nano Energy* 55, 494–500.
- Munday, J.N., 2019. Tackling Climate Change through Radiative Cooling. *Joule* 3 (9), 2057–2060.
- Munday, J.N., Safi, T., 2016. Radiative cooling of a GaAs solar cell to improve power conversion efficiency. In: 2016 IEEE 43rd Photovoltaic Specialists Conference (PVSC), pp. 1125–1127.
- Muselli, M., Beysens, D., Marcillat, J., et al., 2002. Dew water collector for potable water in Ajaccio (Corsica Island, France). *Atmos. Res.* 64 (1), 297–312.
- Nahar, N.M., Sharma, P., Purohit, M.M., 2003. Performance of different passive techniques for cooling of buildings in arid regions. *Build. Environ.* 38 (1), 109–116.
- Nilsson, N.A., Eriksson, T.S., Granqvist, C.G., 1985. Infrared-transparent convection shields for radiative cooling: Initial results on corrugated polyethylene foils. *Solar Energy Materials* 12 (5), 327–333.
- Nilsson, T.M.J., Niklasson, G.A., 1995. Radiative cooling during the day: simulations and experiments on pigmented polyethylene cover foils. *Sol. Energy Mater. Sol. Cells* 37 (1), 93–118.
- Nilsson, T.M.J., Niklasson, G.A., Granqvist, C.G., 1992. A solar reflecting material for radiative cooling applications: ZnS pigmented polyethylene. *Sol. Energy Mater. Sol. Cells* 28 (2), 175–193.
- Nishioka, K., Ota, Y., Tamura, K., et al., 2013. Heat reduction of concentrator photovoltaic module using high radiation coating. *Surf. Coat. Technol.* 215, 472–475.
- NREL-ASTM. Reference Air Mass 1.5 Spectra-ASTM G-173-03 2003; Available from: <https://www.nrel.gov/grid/solar-resource/spectra-am1.5.html>.
- Oak Ridge National Laboratory. Cool roof calculator. [cited 2020 March 18]; Available from: <https://web.ornl.gov/sci/buildings/tools/cool-roof/>.
- Ono, M., Chen, K., Li, W., et al., 2018. Self-adaptive radiative cooling based on phase change materials. *Opt. Express* 26 (18), A777–A787.
- Orel, B., Gunde, M.K., Krainer, A., 1993. Radiative cooling efficiency of white pigmented paints. *Sol. Energy* 50 (6), 477–482.
- Palik, E.D., 1998. Handbook of optical constants of solids. Academic press, p. 3.

- Parker, D.S., 2005. Theoretical evaluation of the night cool nocturnal radiation cooling concept. Submitted to: US Department of Energy. FSEC-CR-1502-05.
- Parker, D.S., Huang, Y.J., Konopacki, S.J., et al., 1998. Measured and simulated performance of reflective roofing systems in residential buildings. *ASHRAE Transactions* 104, 963.
- Parker, D.S., Sherwin, J.R., 2008. Evaluation of the NightCool Nocturnal Radiation Cooling Concept: Annual Performance Assessment in Scale Test Buildings Stage Gate 1B. Florida Solar Energy Center, Cocoa, FL (United States).
- Pisello, A.L., 2017. State of the art on the development of cool coatings for buildings and cities. *Sol. Energy* 144, 660–680.
- Qin, Y., Liang, J., Tan, K., et al., 2016. A side by side comparison of the cooling effect of building blocks with retro-reflective and diffuse-reflective walls. *Sol. Energy* 133, 172–179.
- Qiu, T., Wang, G., Xu, Q., et al., 2018. Study on the thermal performance and design method of solar reflective-thermal insulation hybrid system for wall and roof in Shanghai. *Sol. Energy* 171, 851–862.
- Qu, Y., Li, Q., Cai, L., et al., 2018. Thermal camouflage based on the phase-changing material GST. *Light Sci. Appl.* 7, 26.
- Raman, A.P., Anoma, M.A., Zhu, L., et al., 2014. Passive radiative cooling below ambient air temperature under direct sunlight. *Nature* 515 (7528), 540–544.
- Raman, A.P., Li, W., Fan, S., 2019. Generating Light from Darkness. *Joule* 3 (11), 2679–2686.
- Rephaeli, E., Raman, A., Fan, S., 2013. Ultrabroadband photonic structures to achieve high-performance daytime radiative cooling. *Nano Lett.* 13 (4), 1457–1461.
- Romeo, C., Zinzi, M., 2013. Impact of a cool roof application on the energy and comfort performance in an existing non-residential building. A Sicilian case study. *Energy Build.* 67, 647–657.
- Rossi, F., Castellani, B., Presciutti, A., et al., 2016. Experimental evaluation of urban heat island mitigation potential of retro-reflective pavement in urban canyons. *Energy Build.* 126, 340–352.
- Rossi, F., Morini, E., Castellani, B., et al., 2015. Beneficial effects of retroreflective materials in urban canyons: results from seasonal monitoring campaign. *J. Phys. Conf. Ser.* 655, 012012.
- Safi, T.S., Munday, J.N., 2015. Improving photovoltaic performance through radiative cooling in both terrestrial and extraterrestrial environments. *Opt. Express* 23 (19), A1120–A1128.
- Saitoh, T.S., Fujino, T., 2001. Advanced energy-efficient house (HARBEMAN house) with solar thermal, photovoltaic, and sky radiation energies (experimental results). *Sol. Energy* 70 (1), 63–77.
- Santamouris, M., Feng, J., 2018. Recent Progress in Daytime Radiative Cooling: Is It the Air Conditioner of the Future? *Buildings* 8 (12).
- Savio, P., Rosenzweig, C., Solecki, W.D., et al., 2006. Mitigating New York City's heat island with urban forestry, living roofs, and light surfaces. New York City Regional Heat Island Initiative. The New York State Energy Research and Development Authority, Albany, NY.
- Shi, D., Gao, Y., Guo, R., et al., 2019. Life cycle assessment of white roof and sedum-tray garden roof for office buildings in China. *Sustainable Cities and Society* 46, 101390.
- Shi, Y., Li, W., Raman, A., et al., 2018. Optimization of Multilayer Optical Films with a Memetic Algorithm and Mixed Integer Programming. *ACS Photonics* 5 (3), 684–691.
- Skoplaki, E., Palyvos, J.A., 2009. On the temperature dependence of photovoltaic module electrical performance: A review of efficiency/power correlations. *Sol. Energy* 83 (5), 614–624.
- Sodha, M.S., Singh, U., Srivastava, A., et al., 1981. Experimental validation of thermal model of open roof pond. *Build. Environ.* 16 (2), 93–98.
- Song, J., Qin, J., Qu, J., et al., 2014. The effects of particle size distribution on the optical properties of titanium dioxide rutile pigments and their applications in cool non-white coatings. *Sol. Energy Mater. Sol. Cells* 130, 42–50.
- Sproul, J., Wan, M.P., Mandel, B.H., et al., 2014. Economic comparison of white, green, and black flat roofs in the United States. *Energy Build.* 71, 20–27.
- Strandberg, R., 2015. Heat to electricity conversion by cold carrier emissive energy harvesters. *J. Appl. Phys.* 118 (21).
- Suehrcke, H., Peterson, E.L., Selby, N., 2008. Effect of roof solar reflectance on the building heat gain in a hot climate. *Energy Build.* 40 (12), 2224–2235.
- Suichi, T., Ishikawa, A., Hayashi, Y., et al., 2018. Performance limit of daytime radiative cooling in warm humid environment. *AIP Adv.* 8 (5).
- Sun, K., Riedel, C.A., Wang, Y., et al., 2018. Metasurface Optical Solar Reflectors Using AZO Transparent Conducting Oxides for Radiative Cooling of Spacecraft. *ACS Photonics* 5 (2), 495–501.
- Sun, X., Silverman, T.J., Zhou, Z., et al., 2017a. Optics-Based Approach to Thermal Management of Photovoltaics: Selective-Spectral and Radiative Cooling. *IEEE J. Photovoltaics* 7 (2), 566–574.
- Sun, X., Sun, Y., Zhou, Z., et al., 2017b. Radiative sky cooling: fundamental physics, materials, structures, and applications. *Nanophotonics* 6 (5), 997–1015.
- Sun, Y., Zhou, Z., Jin, X., et al., 2017c. Radiative cooling for concentrating photovoltaic systems. *SPIE Optical Engineering + Applications* 10369, SPIE.
- Synnefa, A., Dandou, A., Santamouris, M., et al., 2008. On the Use of Cool Materials as a Heat Island Mitigation Strategy. *Journal of Applied Meteorology and Climatology* 47 (11), 2846–2856.
- Synnefa, A., Salari, M., Santamouris, M., 2012. Experimental and numerical assessment of the impact of increased roof reflectance on a school building in Athens. *Energy Build.* 55, 7–15.
- Synnefa, A., Santamouris, M., Akbari, H., 2007a. Estimating the effect of using cool coatings on energy loads and thermal comfort in residential buildings in various climatic conditions. *Energy Build.* 39 (11), 1167–1174.
- Synnefa, A., Santamouris, M., Apostolakis, K., 2007b. On the development, optical properties and thermal performance of cool colored coatings for the urban environment. *Sol. Energy* 81 (4), 488–497.
- Syurik, J., Jacucci, G., Onelli, O.D., et al., 2018. Bio-inspired Highly Scattering Networks via Polymer Phase Separation. *Adv. Funct. Mater.* 28 (24).
- Taylor, S., Yang, Y., Wang, L., 2017. Vanadium dioxide based Fabry-Perot emitter for dynamic radiative cooling applications. *J. Quant. Spectrosc. Radiat. Transfer* 197, 76–83.
- Testa, J., Krarti, M., 2017. A review of benefits and limitations of static and switchable cool roof systems. *Renew. Sustain. Energy Rev.* 77, 451–460.
- Tevar, J.A.F., Castaño, S., Marijuán, A.G., et al., 2015. Modelling and experimental analysis of three radioconvective panels for night cooling. *Energy Build.* 107, 37–48.
- Thongtattanasiri, S., Koppens, F.H.L., García de Abajo, F.J., 2012. Complete Optical Absorption in Periodically Patterned Graphene. *Phys. Rev. Lett.* 108 (4), 047401.
- Tikhonravov, A.V., Trubetskoy, M.K., DeBell, G.W., 2007. Optical coating design approaches based on the needle optimization technique. *Appl. Opt.* 46 (5), 704–710.
- Tong, S., Li, H., Zingre, K.T., et al., 2014. Thermal performance of concrete-based roofs in tropical climate. *Energy Build.* 76, 392–401.
- Torgerson, E., Hellhake, J., 2020. Polymer solar filter for enabling direct daytime radiative cooling. *Solar Energy Materials and Solar Cells*, 206.
- Toucheai, A.G., Hosseini, M., Akbari, H., 2016. Energy savings potentials of commercial buildings by urban heat island reduction strategies in Montreal (Canada). *Energy Build.* 110, 41–48.
- Trombe, F., 1967. Perspectives sur l'utilisation des rayonnements solaires et terrestres dans certaines régions du monde. *Rev. Gen. Therm.* 6 (70), 1285–1314.
- University of Wyoming. Upper air data soundings. [cited 2020 17 August]; Available from: <http://weather.uwyo.edu/upperair/sounding.html>.
- Wang, W., Fernandez, N., Katipamula, S., et al., 2018. Performance assessment of a photonic radiative cooling system for office buildings. *Renewable Energy* 118, 265–277.
- Wang, X., Liu, X., Li, Z., et al., 2019. Scalable Flexible Hybrid Membranes with Photonic Structures for Daytime Radiative Cooling. *Adv. Funct. Mater.* 30 (5).
- Wojtysiak, C.S., Butler, J.W., 2009. Radiative cooling surface coatings. Patent US7503971B2 17,03, 2009.
- Wong, N.H., Cheong, D.K.W., Yan, H., et al., 2003. The effects of rooftop garden on energy consumption of a commercial building in Singapore. *Energy Build.* 35 (4), 353–364.
- Wray, C., Akbari, H., 2008. The effects of roof reflectance on air temperatures surrounding a rooftop condensing unit. *Energy Build.* 40 (1), 11–28.
- Wu, D., Liu, C., Xu, Z., et al., 2018. The design of ultra-broadband selective near-perfect absorber based on photonic structures to achieve near-ideal daytime radiative cooling. *Mater. Des.* 139, 104–111.
- Xiong, X., Jiang, S.-C., Hu, Y.-H., et al., 2013. Structured Metal Film as a Perfect Absorber. *Adv. Mater.* 25 (29), 3994–4000.
- Xu, T., Sathaye, J., Akbari, H., et al., 2012. Quantifying the direct benefits of cool roofs in an urban setting: Reduced cooling energy use and lowered greenhouse gas emissions. *Build. Environ.* 48, 1–6.
- Yan, H., Low, T., Zhu, W., et al., 2013. Damping pathways of mid-infrared plasmons in graphene nanostructures. *Nat. Photonics* 7 (5), 394–399.
- Yang, J., Mohan Kumar, D.L., Pyrgou, A., et al., 2018. Green and cool roofs' urban heat island mitigation potential in tropical climate. *Sol. Energy* 173, 597–609.
- Yang, Y., Zhang, Y., 2020. Passive daytime radiative cooling: Principle, application, and economic analysis. *MRS Energy & Sustainability* 7.
- Yu, N., Mandal, J., Overvig, A., et al., 2016. Systems and Methods for Radiative Cooling and Heating. Patent WO/2016/205717 22.12.2016.
- Yu, X., Chen, C., 2020. A simulation study for comparing the cooling performance of different daytime radiative cooling materials. *Solar Energy Materials and Solar Cells*, 209.
- Yuan, J., Emura, K., Farnham, C., 2016. Potential for Application of Retroreflective Materials instead of Highly Reflective Materials for Urban Heat Island Mitigation. *Urban Studies Research* 2016, 1–10.
- Zeyghami, M., Goswami, D.Y., Stefanakos, E., 2018. A review of clear sky radiative cooling developments and applications in renewable power systems and passive building cooling. *Sol. Energy Mater. Sol. Cells* 178, 115–128.
- Zeyghami, M., Stefanakos, E., Goswami, D.Y., 2017. Development of one-dimensional photonic selective emitters for energy harvesting applications. *Sol. Energy Mater. Sol. Cells* 163, 191–199.
- Zhai, Y., Ma, Y., David, S.N., et al., 2017. Scalable-manufactured randomized glass-polymer hybrid metamaterial for daytime radiative cooling. *Science* 355 (6329), 1062–1066.
- Zhan, T.R., Zhao, F.Y., Hu, X.H., et al., 2012. Band structure of plasmons and optical absorption enhancement in graphene on subwavelength dielectric gratings at infrared frequencies. *Physical Review B* 86 (16), 165416.
- Zhan, Z., ElKabbash, M., Li, Z., et al., 2019. Enhancing thermoelectric output power via radiative cooling with nanoporous alumina. *Nano Energy* 65.
- Zhang, K., Zhao, D., Yin, X., et al., 2018. Energy saving and economic analysis of a new hybrid radiative cooling system for single-family houses in the USA. *Appl. Energy* 224, 371–381.
- Zhang, S., Niu, J., 2012. Cooling performance of nocturnal radiative cooling combined with microencapsulated phase change material (MPCM) slurry storage. *Energy Build.* 54, 122–130.
- Zhao, B., Ao, X., Chen, N., et al., 2020a. A spectrally selective surface structure for combined photo-thermic conversion and radiative sky cooling. *Frontiers in Energy*.
- Zhao, B., Hu, M., Ao, X., et al., 2019a. Radiative cooling: A review of fundamentals, materials, applications, and prospects. *Appl. Energy* 236, 489–513.

- Zhao, B., Hu, M., Ao, X., et al., 2017. Conceptual development of a building-integrated photovoltaic–radiative cooling system and preliminary performance analysis in Eastern China. *Appl. Energy* 205, 626–634.
- Zhao, B., Hu, M., Ao, X., et al., 2019b. Performance evaluation of daytime radiative cooling under different clear sky conditions. *Appl. Therm. Eng.* 155, 660–666.
- Zhao, B., Hu, M., Ao, X., et al., 2018. Comprehensive photonic approach for diurnal photovoltaic and nocturnal radiative cooling. *Sol. Energy Mater. Sol. Cells* 178, 266–272.
- Zhao, B., Hu, M., Ao, X., et al., 2020b. Spectrally selective approaches for passive cooling of solar cells: A review. *Appl. Energy* 262.
- Zhao, B., Li, X., Hu, M., et al., 2020c. Consideration of cooling loss process of the emitter for radiative cooling. *J. Renewable Sustainable Energy* 12 (1).
- Zhao, D., Aili, A., Zhai, Y., et al., 2019c. Subambient Cooling of Water: Toward Real-World Applications of Daytime Radiative Cooling. *Joule* 3 (1), 111–123.
- Zhao, D., Aili, A., Zhai, Y., et al., 2019d. Radiative sky cooling: Fundamental principles, materials, and applications. *Appl. Phys. Rev.* 6 (2), 021306.
- Zhao, D., Yin, X., Xu, J., et al., 2020d. Radiative sky cooling-assisted thermoelectric cooling system for building applications. *Energy*, 190.
- Zhou, Z., Sun, X., Bermel, P., 2016. Radiative cooling for thermophotovoltaic systems. SPIE Optical Engineering + Applications 9973, SPIE.
- Zhu, L., Raman, A., Fan, S., 2013. Color-preserving daytime radiative cooling. *Appl. Phys. Lett.* 103 (22).
- Zhu, L., Raman, A., Wang, K.X., et al., 2014. Radiative cooling of solar cells. *Optica* 1 (1).
- Zhu, L., Raman, A.P., Fan, S., 2015. Radiative cooling of solar absorbers using a visibly transparent photonic crystal thermal blackbody. *Proc Natl Acad Sci U S A* 112 (40), 12282–12287.
- Zingre, K.T., Wan, M.P., 2013. An Investigation of Heat Transfer Characteristics of Cool Coating for Building Roofs in the Tropical Climate, ASME 2013 International Mechanical Engineering Congress and Exposition. American Society of Mechanical Engineers, pp. V08AT09A056-V08AT09A056.
- Zingre, K.T., Wan, M.P., Tong, S., et al., 2015a. Modeling of cool roof heat transfer in tropical climate. *Renewable Energy* 75, 210–223.
- Zingre, K.T., Wan, M.P., Yang, X., 2015b. A new RTTV (roof thermal transfer value) calculation method for cool roofs. *Energy* 81, 222–232.
- Zingre, K.T., Yang, X., Wan, M.P., 2014. An Investigation of Microclimatic Impact of Cool Coating for Buildings in Low-Latitude and Tropical Climate, ASME 2014 International Mechanical Engineering Congress and Exposition. American Society of Mechanical Engineers, pp. V06AT07A039-V06AT07A039.
- Zou, C., Ren, G., Hossain, M.M., et al., 2017. Metal-Loaded Dielectric Resonator Metasurfaces for Radiative Cooling. *Adv. Opt. Mater.* 5 (20), 1700460.